Optimizing and Exploring Untapped Micro-Hydro Hybrid Systems: a Multi-Objective Approach for Crystal Lake as a Large-Scale Energy Storage Solution

Sharaf K. Magableh[a]*, Oraib Dawaghreh[a], Caisheng Wang[a]

[a]Department of Electrical and Computer Engineering, Wayne State University, Detriot, United States

Abstract

This paper proposes a method of exploring existing geographic locations with untapped pump hydro storage potentials for accommodating intermittent renewable energy generation profiles. Measured data in 2022 were gathered for sizing system's components and thorough, realistic analysis. Employing a multi-objective grey wolf optimization algorithm, we formulate optimal sizing and energy management strategies for different scenarios. The 1st scenario aims to maximize the reliability objective function (ROF) index of reliability (IR) whilst minimizing the cost objective function (COF) levelized cost of energy (LCOE). The 2nd scenario focuses on maximizing ecological objective function (EOF) CO_2 reduction amount (CO_2RA) whilst minimizing COF, and the 3rd scenario is for maximizing both ROF and EOF while minimizing COF. Considering economic, environmental, and reliability factors as the three objective functions (OFs), has proven to yield promising results in the third scenario when including triple OFs with multiple solutions. A case study is done for the region of Crystal Lake, Michigan. Findings reveal that, although Crystal's Lake would only function as a micro-hydro power facility, it is a promising and huge storage unit with a substantial storage capacity of around 14.9734GWh. These outcomes include a notably low LCOE at 0.046147$/kWh, a robust IR of 99.705%, and a significant reduction in CO_2 emissions amounting to 7.9142×10^3 ton/year, when considering the triple OFs. Validation of the findings was conducted using multi-objective particle swarm optimization algorithms, affirming the robustness of the proposed solutions. The paper's methodology provides valuable insights for regions aiming to utilize renewable energy from untapped storage sources.

Keywords: Fuzzy logic, Levelized cost of energy, Optimal configuration, Pumped hydro storage, Solar photovoltaic array, Triple objective functions.

Nomenclature

Abbreviations	***Meaning***
DDM	Double Diode Model
DHI	Direct Horizontal Irradiance
DNI	Direct Normal Irradiance
EOF	Ecological Objective Function
ESS	Energy Storage System
GHG	Greenhouse Gas Emissions
MHPP	Micro-Hydropower Plant
MGA	Messy Genetic Algorithm
NSRDB	National Solar Radiation Database

* Sharaf K. Magableh. Tel.: +1-313(265)-8254
E-mail address: Sharaf.magableh@wayne.edu

PHESS	Pumped Hydro Energy Storage System
PV	Solar Photovoltaic
RES	Renewable Energy Systems
RERs	Renewable Energy Resources
ROF	Reliability Objective Function
UCL	Upper Crystal Lake

Symbol Name Unit

ACS	Annualized Cost of the System
CC	Capital Cost
CEA	Carbon-Dioxide Emission Amount
COE	Cost of Energy
COF	Cost Objective Function
CRF	Capital Recovery Factor
IR	Index of Reliability
LCOE	Levelized Cost of Energy
LOLP	Loss of Load Probability
LPSP	Loss of Power Supply Probability
GTI	Global Tilted Irradiance
NPC	Net Present Cost
P&L	Transmission and Distribution Line Losses Percentage
OMC	Operation and Maintenance Cost
QOW	Quantity of Water in m^3
RC	Replacement Cost
RSF	Renewable Storage Factor
SC	Salvage Cost
TCC	Total Current Cost
$T_{m_{PV}}$	Solar PV Module Temperature in ℃
T_{amb}	Ambient Temperature in ℃
$NOCT$	Nominal Operating Cell Temperature in ℃
$T_{MDS,STC}$	Manufacturer Data Sheet Temperature at Standard Test Conditions in ℃
v	Hourly Measured Wind Speed in m/s
V_{adj}	Adjusted Wind Speed at Hub Height in m/s
H_{hub}	Hub Height in m
$H_{measured}$	Height at Wind Spead Measured in m
I_{Ph}	Photon Current in Ampere
P_{WT}	Power Extracted from Wind Turbine in MW
N_{WT}	Number of Wind Turbines
P_r	Rated Power in MW
V_{ci}	Cut-in Speed in m/s
V_{co}	Cut-out Speed in m/s
q_p	Pump Flow Rate in m^3/s
q_t	Water Volumetric Flow Rate in m^3/s

E_C	Gravitational Potential Energy
n_{day}	The Duration of Autonomy days
P_{gen}	Power Generated from Hybrid System in MW
$P_{PV\,inv}$	Power Generated Inverted from PV System
P_L	Load Demand in MW
$P_{MHPP_{dis}}$	Generated Power from MHPP Turbines in MW
P_{gp}	Power Grid Purchased in MW
P_{extra}	Extra Generated Power from Hybrid System in MW
$P_{MHPP_{ch}}$	Power Stored in MHPP in MW
P_{gsold}	Power Sold to the Grid in MW
Greek Symbols	
a_w	Wind Power Law Exponent
α_s	Solar Altitude Angle in degree
β_s	Solar Tilted Angle in degree
φ	Latitude Angle in degree
δ	Declination Angle in degree
θ_z	Zenith Angle in degree
ρ	water density ($1000 kg/m^3$)
ρ_o	Air density at sea level, and it is equal to 1.225 kg/m^3
η_T	Efficiency of the hydro turbine (in %)

1. Introduction

Climate change, fossil fuel usage, and energy prices have constantly been top global topics. Based on the current global climate change, energy utilization, and climate policies, it is estimated that the fossil fuel share in global energy will drop from 80% to around 73% by the end of the year 2029 [1]. Hence, the adoption of new sustainable energy technologies will ease the challenges related to energy shortages and balance the energy transition domestically and internationally. As energy is crucial for our lives, in recent decades, hybrid renewable energy systems (RESs) have appeared as a practical solution for supplying electricity to several areas, including remote rural areas where expanding the grid is impractical and extremely expensive [2]. A RES may include several sustainable resources, such as solar photovoltaic, wind energy, micro-hydro, and biomass energy, which can work along with conventional backup generators. In addition to generating clean electricity, large-scale solar, and wind power plants contribute to issues such as environmental waste accumulation and electricity generation intermittence. Therefore, there is a constant and urgent need for clean and dispatchable sources of energy production and storage. Among several RES technologies, hydro power stands out as a promising economic and reliable choice. Indeed, building large-scale hydropower facilities encounters challenges such as ecological impacts and high capital costs, which make them less attractive. Moreover, large-scale, centralized hydropower resources have already been extensively (if not fully) exploited in many countries and regions. Nevertheless, there still exist many untapped pico- and micro-hydro power resources from relatively small rivers and lakes and hydro storages, which show notable potential for long-term electricity generation and storage. For instance, Michigan, a state with thousands of lakes [3], presents a substantial opportunity for micro-hydro projects, in addition to its abundant rivers and high rainfall that serve those storage lakes.

The authors in [4] propose an effective methodology for optimal production benefits for hydropower systems, particularly for installing micro hydropower within water distribution networks. Their methodologies were to investigate technical and economic studies to evaluate practicability and economic feasibility, in terms of optimal sizing using an optimization algorithm. They applied the proposed algorithm to a case study in Morocco's water supply network, including the design and installation of a micro-hydro power plant (MHPP) and considering environmental aspects. Results indicate a substantial cost drop by utilizing existing infrastructures, and an annual average emission reduction of 282 tons, which proves the potential of integrating micro hydropower into water supply systems. They also found the proposed installation is ecologically sustainable and will generate clean energy with an obtained power output of 69 kW. In [5], the researchers discussed an on-grid solar PV combined with MHPP in Unand, Indonesia. This study aimed to find the optimal sizing of micro-hydro hybrid systems to enhance renewable power generation. They implement their system using HOMER software to optimize the head height and flow rate of the MHPP by minimizing the cost of energy (COE). The results showed that the head height was 30m with a flow rate of 800L/s at the lowest value of COE of 0.065 $/kWh. Moreover, the optimal capacity enhances renewable energy generation by a renewable fraction improvement from 26.4% to 36.5%. Reference [6], discussed the availability of renewable energy resources (RERs) in Pakistan as a developing country and how to effectively harness these resources for electricity generation. This is done by introducing an MHPP situated at a specific canal in KPK, Pakistan. The modeling and optimization of the project were implemented using RETScreen software and were thoroughly discussed. The authors compute the net present value (NPV) and the COE using the RETScreen optimization assessment and validate the feasibility of the MHPP. RETScreen simulated a micro-hydro system as a case study with a capacity of 107 kW over a 20-year lifespan. The suggested micro hydropower project is technically applicable and economically viable, with a NPV of $139,280 and a COE of 0.049 $/kWh. The findings revealed that the proposed project will recover all the spending by the 4th year of its planned duration. Notably, when compared to the country's baseline energy mix, the proposed project is identified as clean energy with greenhouse gas (GHG) emission free. To solve the issue of intermittency in RERs due to the natural variations in power generation, which also follow daily and seasonal patterns, it becomes mandatory to combine a complementary energy storage system in those hybrid RERs. A viable alternative for energy storage in hybrid systems is a pumped hydro energy storage system (PHESS). The authors in [7], introduced a technique to represent a PHESS by creating an equivalent battery in HOMER since HOMER didn't have a PHESS component at that time, which was demonstrated through a detailed example. They designed another example consisting of a wind-hydro hybrid power system to validate their methods. The results confirm that the method outlined in their paper effectively represents PHESS for electric energy storage. In order to address energy scarcity challenges such as limited resources which can lead to lower efficiency, especially in sub-generation systems, the researchers in [8] present a design methodology utilizing a customized messy evolutionary approach called the Messy Genetic Algorithm to determine the optimal layout for MHPP. Their methodology considers multiple constraints associated with supply requirements, maximum flow use, and the substantial feasibility of the plant based on the actual geographical profile. This profile allows a continuous, variable-length Messy Genetic Algorithm (MGA) to optimize the layout, by applying two scenarios: cost minimization as a single-objective in one case and minimization of both cost and power supply as a multi-objective in the other case. The algorithm is implemented for a real remote community system in Honduras. Results show that a significant cost reduction of around 56.96% occurred compared to previous designs. On the other hand, considering other boundaries, the MGA was employed to optimize the problem without handling the penstock diameter as a variable. They found that shorter penstocks were created when considering fixed penstock diameter, reaching a 24.22% reduction in length compared to the solution with the optimized diameter, but with significantly higher costs of 285% increase. The PHESS boasts a global installed power capacity of 153GW [9]. This inspires the authors in [10], to introduce a novel Mixed Integer Linear Programming model intended to optimize the operation of such storage plants by maximizing the system's profits. Their model can accommodate a larger number of breakpoints, allowing for more practical solutions with the lowest computational effort. To validate the effectiveness of their model, it was applied to two real plants in the Argentine Republic: the Rio Grande and Los Reyunos power plants, with a combined installed power capacity of 975 MW. The results demonstrate that the suggested model provided feasible solutions with an adequate level of accuracy, within CPU times of less than one second. In [11], the researchers integrated two types of energy storage specifically, MHPP and battery storage, into a small-scale RES. Their study implemented optimal design for off-grid renewable-micro PHESS and battery storage systems in a remote area of Sweden. Their objective was to estimate efficiency, cost, and storage duration. In addition to find the most suitable solution by considering techno-economic performance indicators such as investment cost, life cycle cost, levelized COE (LCOE), and loss of power supply probability (LPSP). The system was optimized using the modified non-dominated sorting Genetic Algorithm. Results reveal that the hybrid PV-wind-battery storage system is the best option in terms of economic benefits and reliability, as the demand is fully satisfied. They found that 18.61% lower life cycle cost and a 6.12% lower oversupply compared to the hybrid PV-wind-micro PHS system. Although this study compared two types of storage, they did not consider the impact of their design on a large-scale hybrid RES. In [12] , the authors provided a practical analysis and sizing of a solar PV system linked with an existing dam as an upper reservoir of the PHESS in Jordan. They explored two scenarios. In the first scenario, they included both RER losses: the losses due to solar PV diffusion and recombination phenomena in the two-diode power model, and the effective head loss in the PHS plant. In the second scenario, they did not consider these types of losses. The system was optimized using particle swarm optimization to determine the optimal value of the index of reliability. They found that to fully cover the load demand, the necessary number of PV panels and the volume of the lower reservoir were to be 44,063 panels and 69.348 Millon m^3, in case no losses are considered, respectively. These values decrease by 14.33% and 5.39% for the second case. Therefore, considering renewable component losses will result in a higher but accurate sizing and prevent undersized design in the case of real system implementation. The authors in [13], proposed a new approach for water and energy management within a wide water supply system, aiming to reduce the costs of energy through the installation of PV plants. They integrate a PHESS to address the intermittency of PV systems. This integrated strategy is applied as a case study to two distinct pumping stations: the "Basso Flumendosa" and the "Monteleone-Roccadoria" pumping stations by maximizing energy self-consumption. Various sizes of PV arrays and hydro turbines are examined to evaluate the obtained self-sufficiency rate and cost performance. The impact of the pumping station's availability for storage purposes was also assessed. The findings indicate that more than 65% of the self-sufficiency rates are attainable only with the integration of the PHESS. A reduction in profitability is observed if full self-sufficiency is achievable for both pumping stations. The researchers in [14], discussed the design of different scenarios for microgrid hybrid RES. They optimized the system by considering multiple objectives, including economic and environmental aspects, namely net percentage cost (NPC) and the reduction of CO_2 emissions. To achieve this, a non-dominated sorting genetic algorithm was implemented to design and optimize the proposed system. The results, when directed toward economic objectives, show the achievement of the lowest energy cost across all scenarios with and without storage units. In contrast, when the optimization technique was centred on environmental objectives, the outcomes indicated a higher overall system cost compared to economic optimization across all scenarios. In [15], the authors discussed a novel tool for creating a penstock layout of MHPP. This proposed procedure depended on a detailed topographic survey of the terrain and used a Genetic Algorithm to optimize the layout of installations. Their mechanism allows for clear integration of several constraints, such as power supply, installation costs, available water flow, and layout feasibility by the actual terrain profile. The algorithm operates in both single-objective mode, aiming to minimize costs, and multi-objective mode, which considers both minimizing cost and maximizing power supply. The application of this algorithm to a real-life case in a distant community in Honduras, Central America, has yielded promising results in terms of generation capacity and cost minimization.

After reviewing existing research and identifying gaps, this paper introduces a new approach: a hybrid renewable energy system (RES) coupled with a utility-scale micro PHESS, as depicted in Fig. 1, to demonstrate and model the proposed methodology. This system integrates solar PV arrays and wind plant installations integrated with the Upper Crystal Lake (UCL) as PHESS. The motivation for this research stems from the limited exploration of MHPP design on a large scale in previous studies, particularly in hydro facilities categorized as MHPPs. Moreover, it aims to address the engineering challenge of integrating hydro facilities with low head heights. Thus, the renewable energy strategy outlined in this paper offers a long-term solution to effectively meet energy demands in Michigan and similar regions globally. Additionally, a double-diode (DD) PV model was employed to ensure precise sizing of the proposed solar system. The proposed mathematical modeling, methodology, optimization algorithm application, and energy management flowchart presented in this paper apply globally to similar cases. In this paper, Crystal Lake's geographical location is utilized as a case study to validate these aspects, employing the realistic measured data for the chosen location in the year 2022, as detailed in Section 2. Multiple multi-objective scenarios were investigated for two and three objectives simultaneously. These scenarios include maximizing power system reliability and reducing CO_2 emissions while minimizing overall system costs. Additionally, the triple Pareto front was simulated to provide a comprehensive view of the combined objective functions for the system's methodology. It is important to note that each scenario yields several solutions, including the best-compromised solution using a fuzzy logic approach. The performance of various renewable energy scenarios is evaluated using a multi-objective approach that considers economic feasibility, reliability, and environmental impacts. This assessment employs a recent multi-objective metaheuristic optimization algorithm, namely the Multi-objective Grew-Wolf optimization algorithm (MOGWOA), to determine optimal system sizing and performance indicators for each scenario, aiming for cleaner energy production. Finally, a comparative analysis is utilized using a multi-objective feasibility-enhanced particle swarm optimization algorithm (MOFEPSOA) to test the effectiveness of MOGWOA. In other words, by comparing the findings obtained using MOFEPSOA, the performance of MOGWOA can be estimated.

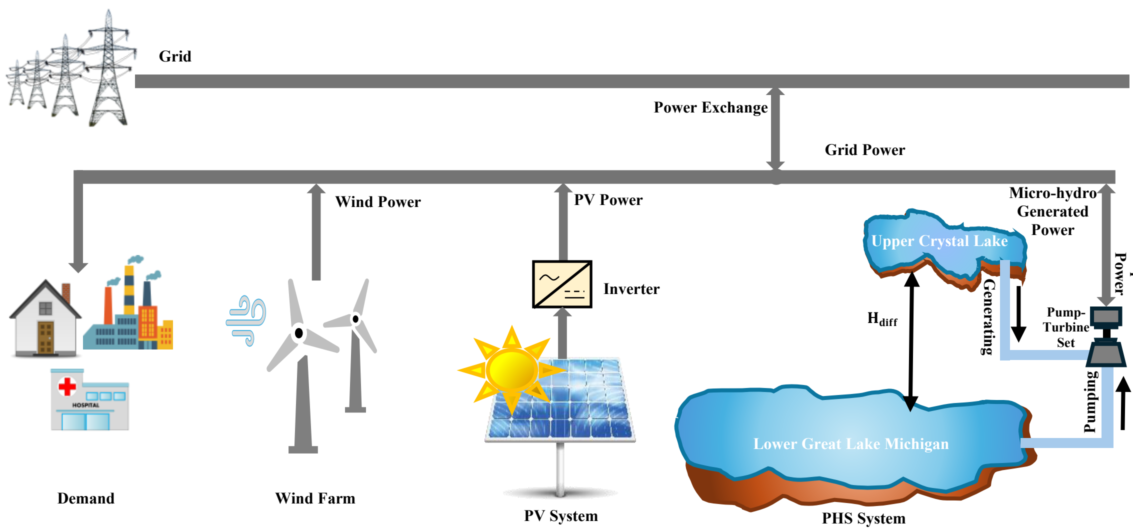

Fig. 1. Schematic diagram of the proposed solar PV and wind power plants combined with the MHPP.

2. System's Realistic Raw and the Corresponding Input Data

The realistic measured data is substantial to accurately design and simulate a real power system and eventually obtain realistic results. This section shows the hourly realistic data for systems' components, including the solar PV system, wind farm, MHPP, and utility-scale load demand for Crystal's Lake territory. It also illustrates the acquired raw and adjusted data that are ready for implementation in the mathematical formulation of the proposed system. Note that, those measured data, i.e., 8760 hours for the year 2022, are obtained from formal US institutions and websites for the proposed geographical location, as explained later in this section.

2.1 Solar PV System Data

The solar PV system data was collected from the National Solar Radiation Database (NSRDB) for the Crystal Lake location [16]. Those data include the hourly measured direct normal irradiance (DNI), diffused horizontal irradiance (DHI), and ambient temperature (T_a). Fig. 2 depicts the hourly DNI and DHI in the Crystal Lake terrain throughout 2022, covering a total of 8,760 hours. It can be noticed that the maximum values of DNI and DHI are 1022W/m^2 and 550W/m^2, respectively, whereas the average values are 171.76W/m^2 and 61.99W/m^2.

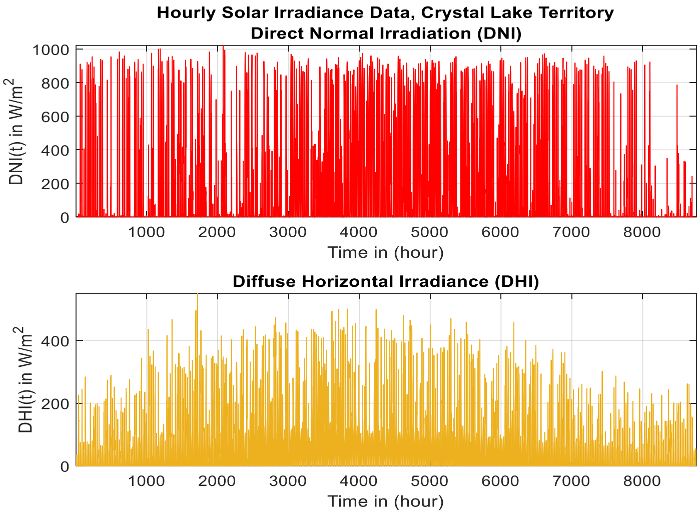

Fig. 2. Hourly measured DNI and DHI values in Crystal Lake terrain in a year.

The data must be converted in the appropriate form in order to be implemented in the double-diode solar PV module presented in section 3.1. Note that, GHI(t) is the total amount of horizontal solar radiation falling on a surface. It is also used to calculate the solar radiation on a tilted surface. GHI resulted in Fig. 3, is mathematically computed based on the hourly raw data of DNI, DHI, and the acquired zenith angle ($\theta_z(t)$) using (1) [17].

$$GHI(t) = DHI(t) + DNI(t) \times \cos(\theta_z(t)) \tag{1}$$

Now, the global tilted solar irradiance ($GTI(t)$) is ready to be computed and entered in the modeling of a solar PV module, as will be explained later in section 3.1. Note that, GTI, shown in Fig. 3, is calculated at each time step using (2) [18].

$$GTI(t) = GHI(t) \times \frac{\sin(\alpha_s(t)+\beta_s)}{\sin(\alpha_s(t))}. \tag{2}$$

Where α_s is computed as in (4), and it depends on the latitude angle (φ) and the declination angle (δ) as in (3). β_s is 37° for Crystal Lake territory [19]. φ is 44.668677° based on the selected site coordinates, and n is the number of days within a year, ranging from 1 to 365. This iteration allows (δ) to vary as a function of the specific day of the year[20].

$$\delta(t) = 23.45^{\circ} \sin\left[\frac{360}{365}(n + 284)\right] \tag{3}$$

$$\alpha_s(t) = 90 - \varphi + \delta(t) \tag{4}$$

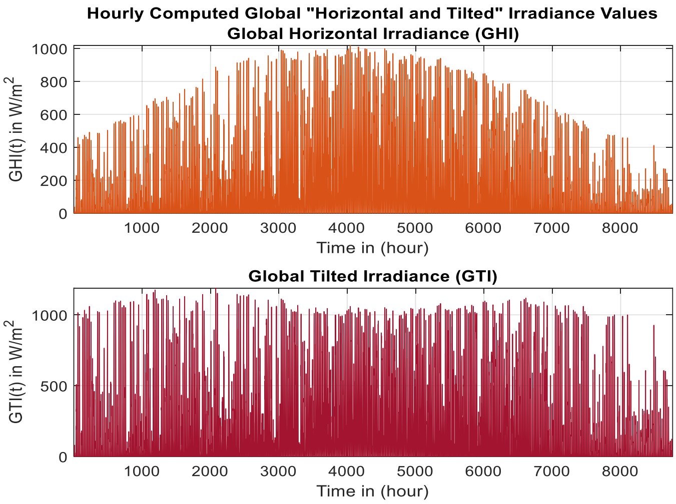

Fig. 3. Hourly measured GHI and computed GTI solar values for Crystal Lake terrain in a year.

The module temperature ($T_{m_{PV}}(t)$) are calculated as in (5) and (6). $T_{amb}(t)$ in (5) is the hourly air ambient temperature obtained from NSRDB [16], and it is converted to $T_{m_{PV}}(t)$ as illustrated in Fig. 4. The selected solar PV is “CanadianSolar All-Black CS6K-290MS” with rated power of 290 Watt. The complete required data and the value of NOCT, $T_{MDS,STC}$ and GTI_{NOCT} are given in Appendix A.

$$T_{m_{PV}}(t) = T_{amb}(t) + \frac{(NOCT - T_{MDS,STC}) \times \mathrm{GTI}(t)}{GTI_{NOCT}} \tag{5}$$

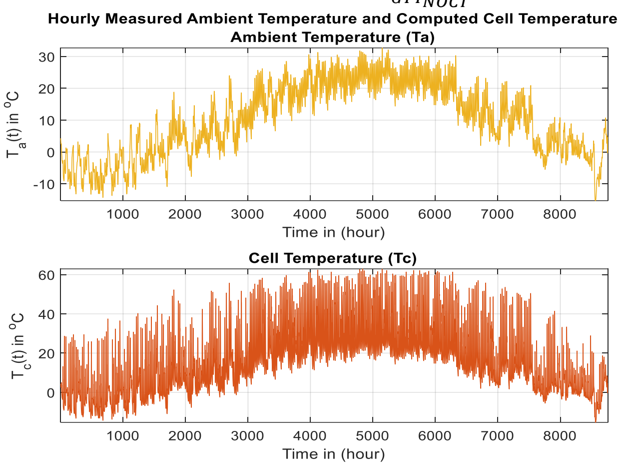

Fig. 4. Hourly measured ambient and computed module temperature values for Crystal Lake terrain.

2.2 Wind Turbine Data

The hourly measured wind speeds $v(t)$, shown in Fig. 5, are obtained from the Weather API [21]. $v(t)$ are fluctuating between 0.42m/s and 18.2 m/s. Before these data can be utilized in the mathematical formulation of wind turbine output power discussed in section 3.2, it is required to calibrated this data according to the hub height (H_{hub}) as in (6) [22].

$$V_{adj}(\mathrm{t}) = v(t) \times \left(\frac{H_{hub}}{H_{measured}}\right)^{a_w} \tag{6}$$

The wind power law exponent, denoted by (a_w), relates the wind speed measured at the H_{hub} of a wind turbine (V_{adj}) to the wind speed measured by an anemometer at $H_{measured}$, as expressed in Equation (6). In addition, empirical studies suggest that a_w is equivalent to 1/7, typically provides the best fit for most sites, see Appendix A. The average wind speed has increased from around 5.28 m/s to 8.11 m/s, as in Fig. 5, after considering the hub height for the proposed wind turbine.

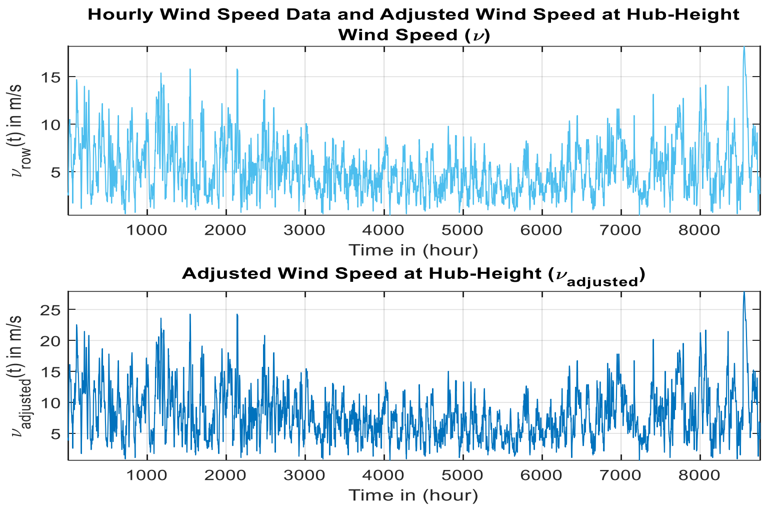

Fig. 5. Hourly measured and computed wind speed values for Crystal Lake terrain.

2.3 Hydropower Plant and Crystal Lake Data

Crystal's Lake history is greatly constrained to several geological shifts in the past as it was initially formed as part of glacial Lake Algonquin around 11,000 years ago [23]. It was found perched 11.5824 m overhead of present-day Lake Michigan at an elevation of around 187.452 m after the glacier's retreat, presenting exposed terraces and flooded shoals along its shoreline [24]. In 1873, the lake witnessed a considerable drop in its levels due to a critical storm that faded and swept away a temporary dam during an attempt to build a canal to Lake Michigan. This event created new beach areas and set the stage for the development of the surrounding region, including a network of roads and trails and the establishment of a resort community. Over the years, the water levels fluctuated due to several issues, which resulted in a subsequent drop of water and a net volume loss of approximately 1.93 million m^3 with an about 6 m drop in head height. However, in the late 18th century, it rebounded again and reached a height of around 183 m, the same as its current level. Hence, the lake's area changed, creating beach zones and impacting its overall features. Crystal Lake became one of the first in Michigan to set a "natural level" at 600.48 feet (183 m). An automatic gauge installed in 2014 helps record lake levels, contributing to the moderation of seasonal changes [25]. It is important to mention that the lake's level plays a pivotal role in defining the water body. The lake is primarily replenished by precipitation and groundwater; therefore, its water level remains relatively independent of Lake Michigan.

In this paper, UCL, depicted in Fig. 6, is designated as the upper reservoir for the MHPP, as illustrated previously in the proposed system in Fig. 1. With a substantial water capacity of around 1.93 million cubic meters, UCL inspires this study to investigate the potential of how lakes of this size function as efficient energy storage systems (ESS). In addition to focusing on the capability of generating electricity within such MHPPs, this research delves into the capacity of lakes like UCL to store energy effectively. Further details regarding UCL can be found in Appendix A [26].

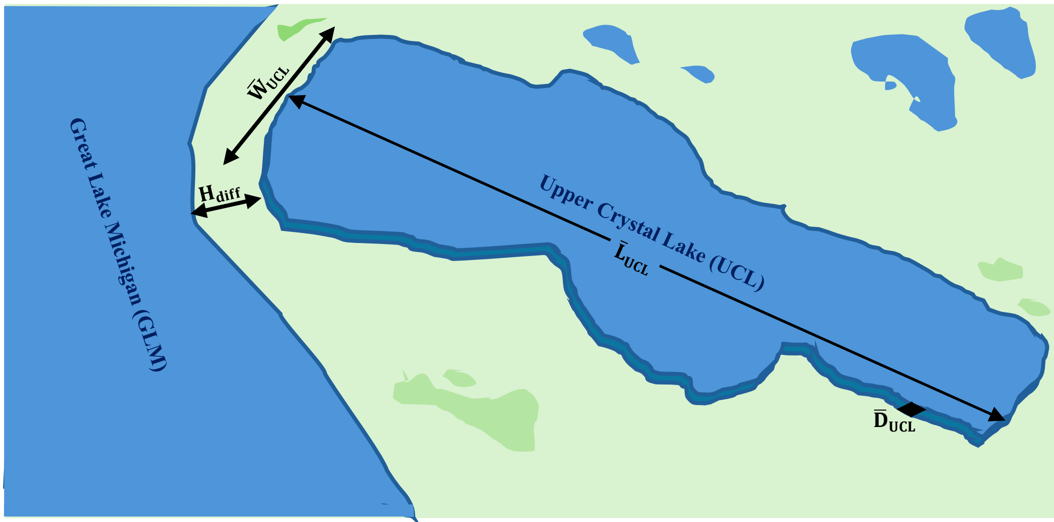

Fig. 6. Geographical representation of the UCL reservoir and the surrounding territory [26].

2.4 Load Demand Data

The load demand data, sourced from UtilityAPI, represents measurements in megawatts (MW) supplying a residential consumers in Benzie County, Michigan [27]. The observed load demand fluctuates within a range spanning from 1.2552 MW to 2.2104 MW, as depicted in Fig. 7.

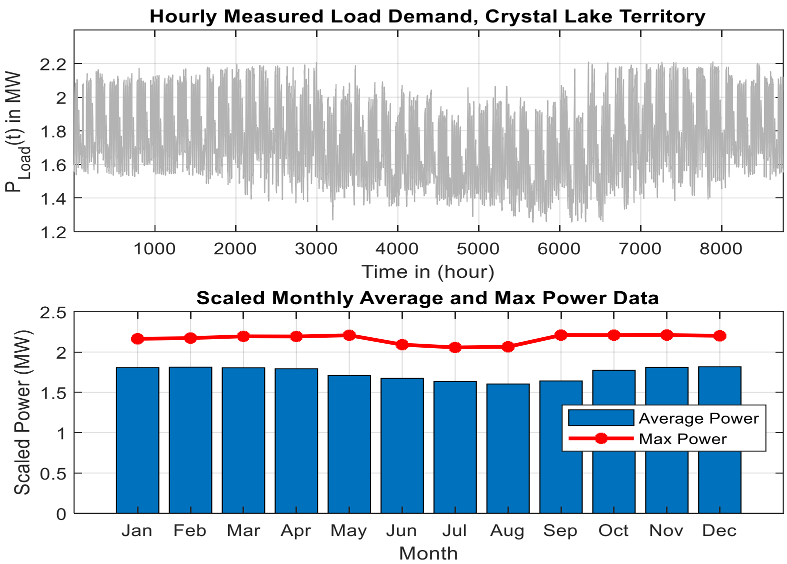

Fig. 7. The hourly measured demand for a 22 kV sub-feeder.

Notably, in Michigan, residential energy usage tends to spike during the winter months compared to the summer. This trend is driven by the cold temperatures experienced during winters, prompting residents to heavily utilize heating systems such as furnaces and boilers to maintain indoor warmth. The increased demand for heating results in peak electricity usage in households during this season. On the other hand, during the summer, although air conditioning usage may rise to beat the heat and humidity, overall electricity demand from homes usually does not hit the same heights as in the winter. It can be noticed that the monthly average demand is within a narrow range of around 1.7389MW during the year, as depicted in Fig. 7.

3. Mathematical and Design Formulation

Mathematical modeling serves as the cornerstone and initial phase for precisely simulating and optimizing the proposed system. Accurate modeling is crucial for determining the appropriate configurations of the systems involved. For the renewable components, a quality factor-based model is utilized for the solar PV array, while a cubic function is chosen to model the wind farm, accounting for parameters such as the wind power coefficient and tip speed ratio. These models rely on input data presented in Section 2. The energy management strategy, depicted in Fig. 8, guides the precise sizing and optimization of the system using MOGWOA.

3.1 Modeling of Solar PV Output Power

In this paper, the double-diode model (DDM) will be utilized to simulate the solar PV module. DDM is commonly used for representing the behaviour of solar PV modules. However, DDM has rarely been implemented in utility applications because of its large computation time and its complexity. This is because it considers all types of losses in the modeling of solar PV module. Nonetheless, DDM gives a more accurate and realistic description of the electrical characteristics of a solar cell compared to other types of solar models, i.e., the single-diode model or the ideal single diode model. Hence, implementing this DDM leads to a true sizing of the PV array and hence, the size and cost of the entire system [28]. The first diode (D_1) represents the diffusion process whilst the second diode (D_2) simulates the recombination phenomena [29]. In other words, D_1 reflects how minority carriers diffuse into the depletion layer, while D_2 mimics the recombination within the junction's space charge region [30]. Therefore, the DDM takes into account solar losses comprehensively, including diffusion, recombination, leakage to ground losses (R_{sh}), and series losses (R_s) as shown in Fig. 8.

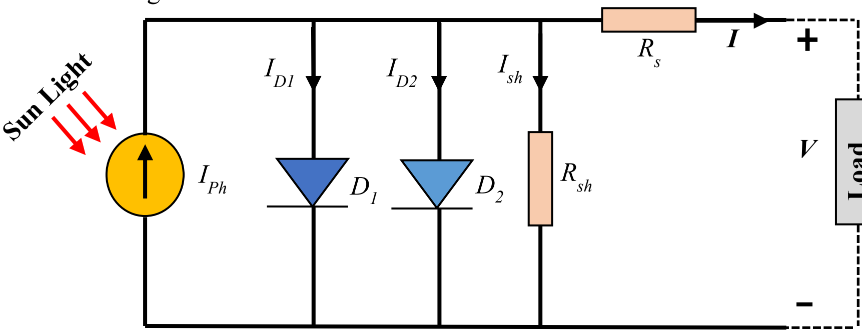

Fig. 8. Equivalent circuit of a two-diode PV module

The DDM gives a more precise and realistic output current from the cell compared with the simpler single-diode model. This is due to considering the recombination process, i.e., D_2 current (I_{D2}) as depicted in equation (7) [31]. I_{D1} , I_{D2} and I_{Sh} are computed as in (8), (9) and (10), respectively [32, 33].

$$I = I_{Ph} - I_{D1} - I_{D2} - I_{Sh} \tag{7}$$

$$I_{D1} = I_{o_1}\left(e^{\left(\frac{V+IR_S}{\alpha_1 V_T}\right)} - 1\right) \tag{8}$$

$$I_{D2} = I_{o_2}\left(e^{\left(\frac{V+IR_S}{\alpha_2 V_T}\right)} - 1\right) \tag{9}$$

$$I_{Sh} = \frac{V+IR_S}{R_{sh}} \tag{10}$$

After substituting (8), (9), and (10) in (7), equation (11) is resulted. The photon current (I_{Ph}) as shown in Fig. 8 and Equ. (11) affects by varying solar irradiance and temperature according to equation (12) [34]. The diode saturation currents I_{o_1} and I_{o_2} depend on temperature and can be expressed as given in (13). Where E_g in (13) represents the band gap energy of the semiconductor and $I_{o,STC}$ is the nominal saturation current at (STC) and can be expressed by (14).

$$I = I_{Ph} - I_{o_1}\left(e^{\left(\frac{V+IR_S}{\alpha_1 V_T}\right)} - 1\right) - I_{o_2}\left(e^{\left(\frac{V+IR_S}{\alpha_2 V_T}\right)} - 1\right) - \frac{V+IR_S}{R_{sh}} \tag{11}$$

$$I_{Ph} = \left[I_{pv_{STC}} + K_I\,(T - T_{STC})\right]\frac{GTI}{G_{STC}} = I_{pv_{STC}}(1 + \alpha_{Isc}\,\Delta T)\,\frac{GTI}{G_{STC}} \tag{12}$$

$$I_o = I_{o,STC}\left(\frac{T_{STC}}{T}\right)^3 exp\left(\frac{qE_g}{\alpha K}\left(\frac{1}{T_n} - \frac{1}{T}\right)\right) \tag{13}$$

$$I_{o_{STC}} = \frac{I_{sc_{STC}}}{\exp\left(\frac{V_{oc_{STC}}}{\alpha\, V_{T_{STC}}}\right) - 1} \tag{14}$$

From the previous two equations (13) and (14), I_o can be expressed as given in (15). As the diode saturation current is very small, to simplify the model, the reverse saturation currents, I_{o_1} and I_{o_2} are set to be equal as in (16) [31]. As α_1 and α_2 in equation (16) are the diode ideality factors that represent the diffusion and recombination effects. Referring to Shockley's diffusion theory, α_1 must be unity while the value of α_2 is varying. If the value of α_2 is in the range of $1.2 \leq \alpha_2 \leq 2$, the best match between the proposed model and the practical I-V curve is obtained according to the simulation results. Hence, $\frac{\alpha_1+\alpha_2}{P} = 1$ and α_1=1. It follows that the variable P can be chosen to be within $2.2 \leq P \leq 3$. Hence, considering these constraints, (16) becomes as in (17) [35].

$$I_o = \frac{I_{sc_{STC}} + K_I\,\Delta T}{\left[exp\left(\frac{V_{oc_{STC}} + K_V\,\Delta T}{V_T * \alpha}\right)\right] - 1} \tag{15}$$

$$I_{o_1} = I_{o_2} = \frac{I_{sc_{STC}} + K_I\,\Delta T}{\left[\exp\left(\frac{V_{oc_{STC}} + K_V\,\Delta T}{V_T\,(\alpha_1+\alpha_2)/P}\right)\right] - 1} \tag{16}$$

$$I_{o_1} = I_{o_2} = \frac{I_{sc_{STC}} + K_I\,\Delta T}{\left[\exp\left(\frac{V_{oc_{STC}} + K_V\,\Delta T}{V_T}\right)\right] - 1} = I_o \tag{17}$$

3.2 Mathematical modeling of Wind Farm

The power extracted from wind turbines (P_{WT}) can be expressed as in (18). Note that, it depends on local wind speed ($V(t)$), the number of wind turbines (N_{WT}), and the parameters of the manufactured wind turbine, such as the rated power in kW (P_r), cut-in speed (V_{ci}) in m/s, and cut-out speed (V_{co}) in m/s [36].

$$P_{WT} = \begin{cases} 0 & , V((t) < V_{ci} \\ \frac{N_{WT}\,P_r(V(t)^3 - V_{ci}^3)}{(V_r^3 - V_{ci}^3)} & , V_{ci} < V(t) < V_r \\ N_{WT}\,P_r & , V_r < V(t) < V_{co} \\ 0 & , \ V(t) > V_{co} \end{cases} \tag{18}$$

3.3 Mathematical Modeling of Micro-Hydro and PHESS

MHPP can be in different types such as dam, run-off-river, and PHESS, or a combination of them. In this study, the MHPP will be in the form of PHESS. The PHESS system operates as a giant battery to store energy. They can store energy as a form of potential energy by pumping the water from the lower reservoir (i.e., Lake Michigan) to the upper Crystals Lake (UCL) reservoir, shown in Fig. 6. This process is called pumping mode. When the hybrid system comprised of solar PV and wind turbines cannot sufficiently meet the load demand, the water is released from the UCL to the lower reservoir, in the process of generating mode.

3.3.1. Pumping (or Charging) Mode

The pump flow rate ($q_p(t)$) from the lower reservoir to UCL is expressed as in Equation (19). It is the relation of surplus or extra power from the hybrid system ($P_{MHPP_{ch}}(t)$) in kW, pump efficiency (η_p), head height (h) in *m*, water density (ρ) ($1000 kg/m^3$), and gravity acceleration (g) ($9.8 m/s^2$) [37].

$$q_p(t) = \frac{\eta_p \, \mathrm{P}_{\mathrm{MHPP_{ch}}}(t)}{\rho g h} \tag{19}$$

3.3.2. Generating (or Discharging) Mode

The released power from the UCL is used to spin the turbine/generator set when the solar PV and wind turbine renewable facilities cannot meet the load demand, and this power can be computed as in (20) [37]. Note that, η_t is the efficiency the turbine/generator set and $q_t(t)$ is the water volumetric flow rate in m^3/s.

$$P_{\mathrm{MHPP}_{dis}}(t) = \eta_t \times \rho \times g \times h \times q_t(t) \tag{20}$$

3.3.3. Upper Crystal Lake (UCL) Reservoir

The quantity of water (QOW) stored in the UCL at any time (*t*) is expressed as in (21) [37]. The QOW in the UCL is governed by the constraints as explained in (22), as the upper and lower safety limit. α is the loss factor from evaporation and leakage to ground. In this paper, α will be considered zero due to the massive volume of UCL.

$$QOW_{\mathrm{UCL}}(t) = QOW_{\mathrm{UCL}}(t-1)(1-\alpha) + q_p(t) - q_t(t) \tag{21}$$

$$QOW_{UR_{min}} \leq QOW_{UR} \leq QOW_{UR_{max}} \tag{22}$$

3.3.4. Storage Capacity

The UCL must have sufficient water stored to meet the power requirements of the demand during extended power outages [38]. The water level (QOW) in the UCL essentially acts as the state of charge explained before for the storage tank. The gravitational potential energy (E_C) in kWh stored in the UCL can be measured as in (23) [39], where V stands for the volume or storage capacity of the water reservoir in cubic meters (m^3).

$$E_C = \frac{\mu_t \times \rho \times V \times g \times h}{3.6 \times 10^6} \tag{23}$$

Based on the planned capacity of the UCL, and the daily energy consumption by the load (E_{Load}) in (kWh), the duration of autonomy days (n_{day}) can be determined by assessing the potential energy stored in the UCL. This calculation can be performed using the following formula (24) [34].

$$n_{day} = \frac{E_C}{E_{Load}} \tag{24}$$

4. System's Operational Flow Chart

Fig. 9 illustrates the operational flow chart and energy management system. This flow chart explains the priority and the flow of energy within the system to meet the load demand. It begins with the power generated by the solar PV and wind plants, followed by the MHPP, and is then sourced from the grid. It also provides a general overview of the algorithm's functionality to optimally design the system.

If the power generated from the hybrid system ($P_{gen}(t)$), as defined in (25), originating from both the PV system ($P_{PV_{inv}}(t)$) as in (26) and wind farm ($P_{WT}(t)$) as specified in (18), is insufficient to satisfy the load demand ($P_L(t)$) presented in section 2.4, the needed load will be covered by generating power during discharging mode from the MHPP facility ($P_{MHPP_{dis}}(t)$). Hence, if $P_{gen}(t)$ and $P_{MHPP_{dis}}(t)$ are still inadequate to meet the load demand, the grid feeds the load demand ($P_{gp}(t)$) as outlined in (27). On the other hand, in the event of extra power generated from the hybrid system ($P_{extra}(t)$) as in (28), then this power is stored in MHPP by pumping the water from the lower reservoir to the UCL ($P_{MHPP_{ch}}(t)$) if and only if the QOW in the UCL is less than the QOW_{max}, if not, the QOW is at the maximum limit, and the extra power is sold to the grid ($P_{gsold}(t)$) [11, 12].

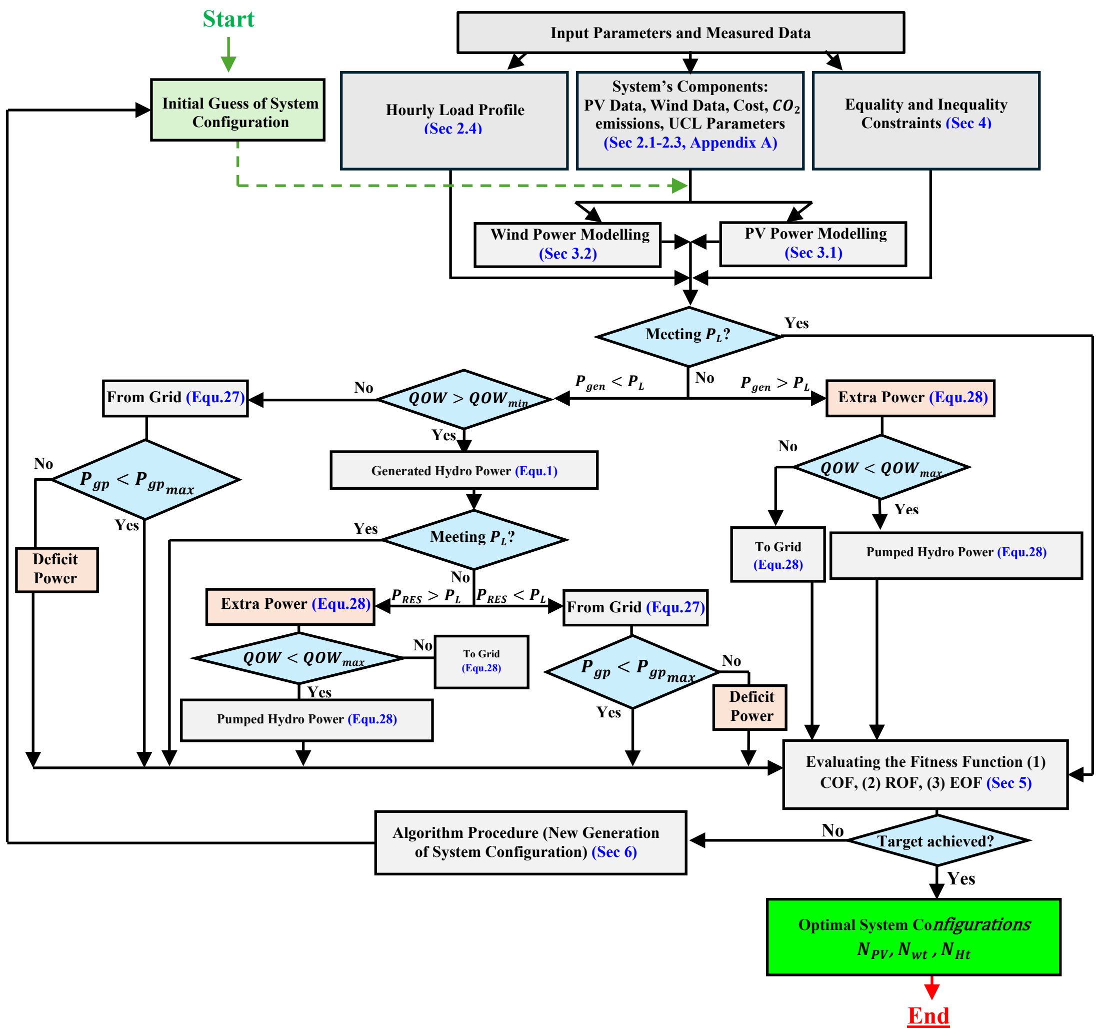

Fig. 9. Energy management strategy and Operational flowchart.

The multi-objective function is assessed at each time step, as shown in Fig. 9. In the case that the maximum power obtained from all renewables covers the load demand and increases, but the grid capacity limit is reached, then the extra power will be directed to a dummy load. In scenarios where the power produced from all renewables and the grid purchased are insufficient to satisfy the load demand, then there is a deficit power ($P_{deficit}(t)$) as depicted in the balance power equation in (28) [11, 12].

$$P_{gen}(t) = P_{PV_{inv}}(\text{t}) + P_{WT}(t) \tag{25}$$

$$P_{PV_{inv}}(\text{t}) = \eta_{inv} \times P_{PV}(t) \times f_{PV} \tag{26}$$

$$P_{gp}(t) = P_L(t) - (P_{gen}(t) + P_{\text{MHPP}_{dis}}(t)) \ , if \ \ P_{gp}(t) \leq P_{gp}(t)_{\text{max}} \tag{27}$$

$$P_{extra}(t) = P_{gen}(t) - P_L(t) = \begin{cases} P_{MHPP_{ch}}(t) & , QOW < QOW_{max} \\ P_{gsold}(t) & , QOW \geq QOW_{max} \end{cases} \tag{28}$$

$$P_{gen}(t) + P_{\text{MHPP}_{dis}}(t) + P_{gp}(t) = P_L(t) + \text{P}_{\text{MHPP}_{\text{ch}}}(t) + P_{gsold}(t) + P_{deficit}(t) \tag{29}$$

5. System's Multi-Objective Functions and *Performance Evaluators*

This section discusses the multi-objective functions that govern the performance of the system and other performance indictors to be computed for each case scenario. In this paper, there are three multi-objective scenarios, including economic aspects versus reliability in one case, ecological and cost impacts in the second case scenario, and all objective functions in the 3rd scenario. The 1st multi-objective function scenario will consider minimizing the levelized cost of energy (LCOE) and maximizing the index of reliability (IR) using the Multi-Objective Grey Wolf Optimizer (MOGWO) algorithm to find the best optimal solution. However, minimizing the LCOE and maximizing the carbon-dioxide reduction amounts (CO_2RA) will be taken into account for the 2nd case scenario. In the 3rd scenario, IR and CO_2RA will be maximized, and LCOE will be minimized as a triple objective function.

The set of solutions in the optimized multi-objective function, namely Pareto front solutions, will provide all types of solutions, including affordable, reliable, and ecological solution sets. For instance, if the designer focuses on the system to be more economic, the set of solutions closer to the minimal cost would be better regardless of the reliability and so on. Note that the optimal configuration of the system depends on the multi-objective function or the best decision variables, including the number of PV panels (N_{PV}), the number of wind turbines (N_{wt}), and the number of hydro-turbine units (N_{Ht}).

5.1. Cost Objective Function (COF)

The LCOE is a mathematical estimation process used in the energy business to calculate the average cost of generating one unit of electricity during the system's lifetime. It considers several parameters, including initial capital costs, operations and maintenance expenses, fuel costs, and the system's projected lifespan energy production.

The COF of LCOE will be minimized, and it is considered as the 1st objective function. It is noted that the computation of the LCOE involves dividing the Annualized Cost of the System (ACS) by the energy supplied to meet the load demand (EL), as illustrated in equation (30). The ACS is derived by multiplying the Total Current Cost (TCC) with the Capital Recovery Factor (CRF). TCC is computed by summing the discounted values of various costs in the system, including Capital Cost (CC), Operation and Maintenance Cost (OMC), Replacement Cost (RC), and Salvage Cost (SC). The CRF is determined by (31), while the real interest rate (i) is found using (32) depending on i'representing the nominal interest rate and the inflation rate (f_{inf}). Appendix B provides the cost values for each component, including their respective lifetimes, along with the financial parameters required for constructing both nominal and discounted cashflows [40].

$$LCOE = \frac{ACS}{E_s} \tag{30}$$

$$CRF = \frac{i(1+i)^N}{(1+i)^N - 1} \tag{31}$$

$$i = \frac{i' - f_{inf}}{1 + f_{inf}} \tag{32}$$

5.2. Reliability Objective Function (ROF)

The Index of reliability (IR) refers to the system's ability to satisfy the load demand, mentioned in section 2.4, without any interruptions or deficit in energy. The 2nd ROF is to be maximized and can be computed as in (33) [41].

$$IR = 1 - \frac{\sum_{t=1}^{8760}[P_L(t) - (P_{PV_{inv}}(t) + P_{WT}(t) + P_{MHPP_{dis}} + P_{gp}(t))]}{\sum_{t=1}^{8760} P_L(t)} \tag{33}$$

5.3. Ecological Objective Function (EOF)

Carbon-Dioxide Reduction Amount (CO_2RA) stands for the reduction in harmful emissions achieved by the utilization of renewable energy resources ($E_{R_{gen}}$) rather than the conventional fossil fuels, as indicated in equation (34) [42]. F_{CO_2}represents the carbon dioxide emission factor, and it is estimated to be 0.553 tCO2/MWh in the context of Michigan [43]. The 3rd EOF of CO_2RA is maximized using MOGWO algorithm as explained in sections 6 and 7.

$$CO_2RA = E_{R_{gen}} \times F_{CO_2} \tag{34}$$

5.4. Complete constrained objective function formulation

The system optimization and sizing are determined by decision variables and a set of equality and inequality constraints, as outlined in Equ. (35) [44]. These decision variables include the number of PV panels (N_{PV}), the number of wind turbines (N_{WT}) and the number of hydro-turbine units (N_{Ht}).

$$\begin{cases} COF: Min\left(LCOE = \frac{ACS}{E_s}\right) \\ ROF: Max\left(IR = 1 - \frac{\sum_{t=1}^{8760}[P_L(t) - (P_{PV_{inv}}(t) + P_{WT}(t) + P_{MHPP_{dis}} + P_{gp}(t))]}{\sum_{t=1}^{8760} P_L(t)}\right) \\ EOF: Max\left(CO_2RA = E_{R_{gen}} \times F_{CO_2}\right) \\ (COF\& \ and \ ROF) \parallel (COF \ and \ EOF) \parallel (COF \ \&ROF \ \& \ EOF) \\ N_{PV}, N_{WT}, N_{Ht} \\ \quad Subject \ to \\ \begin{cases} P_{gp}(t) \le P_{gp_{max}} \\ QOW_{min} \le QOW(t) \le QOW_{max} \\ P_{extra}(t) = P_{gen}(t) - P_L(t) = \begin{cases} P_{MHPP_{ch}}(t), QOW < QOW_{max} \\ P_{gsold}(t) \quad , QOW \ge QOW_{max} \end{cases} \\ P_{gp}(t) = P_L(t) - \left(P_{gen}(t) + P_{MHPP_{dis}}(t)\right) \\ P_{gen}(t) + P_{MHPP_{dis}}(t) + P_{gp}(t) = P_L(t) + P_{MHPP_{ch}}(t) + P_{gsold}(t) + P_{deficit}(t) \end{cases} \end{cases} \tag{35}$$

5.5. Other Performance Evaluators

This section shows other appropriate performance indicators to assess the behavior of the system at an optimal solution of each scenario. This includes estimating the Loss of Load Probability (LOLP), Carbon-Dioxide Emissions Amount (CEA), and Renewable Storage Factor (RSF).

LOLP serves as a metric to assess the number of hours in a given year during which the system falls short of meeting the load requirements, as indicated in equation (36). A lower LOLP value indicates a higher level of reliability in the system. Essentially, LOLP delves into the hours when the system experiences inadequacy in meeting the load demand or encounters a power deficit [45].

$$LOLP = \frac{\sum_{t=1}^{8760} h[\,P_L(t) > (P_{PV_{inv}}(t) + P_{WT}(t) + P_{MHPP_{dis}} + P_{gp}(t))]}{8760} \tag{36}$$

CEA is a measure of the greenhouse gas emissions (GHGEs), primarily CO_2, released when relying on the utility grid, as specified in equation (37) [42]. This quantity is related to the CO_2 emission factor (F_{CO_2}), mentioned before. Additionally, it factors in the losses percentage in transmission and distribution lines (PL), with Michigan registering approximately 5% in this regard [46]. Notably, a lower CEA value signifies a more efficient utilization of renewable energies, highlighting the environmental benefits associated with reduced carbon emissions.

$$CEA = \frac{E_{gp} \times F_{CO_2}}{1-PL} \tag{37}$$

RSF gauges the extent to which the energy supplied by the UCL of the MHPP facility fulfills the overall demand, as expressed in equation (38) [47]. Here, $E_{Storage}$ represents the energy conveyed to the load by PHS, while E_{System} encompasses the energy output of the entire system, inclusive of MHPP.

$$RSF = \sum_0^t \frac{E_{Storage}}{E_{System}} \tag{38}$$

6. System's Multi-Objective Optimization Algorithms

This research employs two multi-objective algorithms to simulate the proposed system. Initially, the MOGWOA is adapted to model the system, incorporating various multi-objective scenarios. This involves modifying the algorithm to minimize system costs while maximizing reliability and ecological considerations. Subsequently, the MOFEPSOA is utilized to validate the results obtained from the MOGWOA. It is important to note that each scenario yields multiple solutions, including reliable, ecological, economic, and optimal compromise solutions, based on the preferences of the designers. The optimal solution, balancing all objectives, is determined using a fuzzy logic approach, as detailed in section 7.

6.1. Multi-objective Grew-Wolf optimization algorithm (MOGWOA)

Mirjalili and Lewis introduced the Grey Wolf Optimizer (GWO) algorithm, which was originally inspired by the social leadership and hunting strategies of grey wolves. The MOGWOA incorporates a fixed-size external archive into the GWO, which enables the storage and retrieval of Pareto optimal solutions. This archive plays a crucial role in establishing a social hierarchy and emulating the hunting behavior of grey wolves in multi-objective search environments. It is worth mentioning that the MOGWOA algorithm was used to solve multi-objective optimization problems, as it is preferred in research for its simplicity and ability to adaptively tune parameters. Many studies, as in [48-52], recommend MOGWOA for tackling complex optimization challenges. Consequently, we employed MOGWOA in this article. For instance, in [53], the primary aim of the proposed MOGWO was to optimize the switching matrix structure to minimize row current differences and maximize output power. This method effectively addressed the challenge of adjusting objective function weights to ensure system reliability and efficiency. The comparison demonstrated MOGWO's superiority in handling multi-peak issues in P-V characteristics, achieving the highest power levels.

When formulating the social hierarchy within the GWO, the most appropriate solution is designated as the alpha (α) wolf. Subsequently, the second and third best solutions are identified as the beta (β) and delta (δ) wolves respectively as shown in Fig. 10. All other candidate solutions are classified as omega (ω) wolves. Within the GWO algorithm, the optimization process is directed by α, β, and δ wolves, while ω wolves follow their lead in the pursuit of the global optimum. Appendix C imitates the encircling behavior equations observed in grey wolves during hunts [54]. It observed that *t* denotes the present iteration, while $\vec{A}$ and $\vec{C}$ represent coefficient vectors. $\vec{X}_p$ refers to the position vector of the prey and $\vec{X}$ signifies the position vector of a grey wolf. The elements of the coefficient vector $\vec{a}$ linearly decrease from 2 to 0 throughout the iterations. Additionally, $\vec{r}_1$ and $\vec{r}_2$ denote random vectors within the range of [0,1] [55].

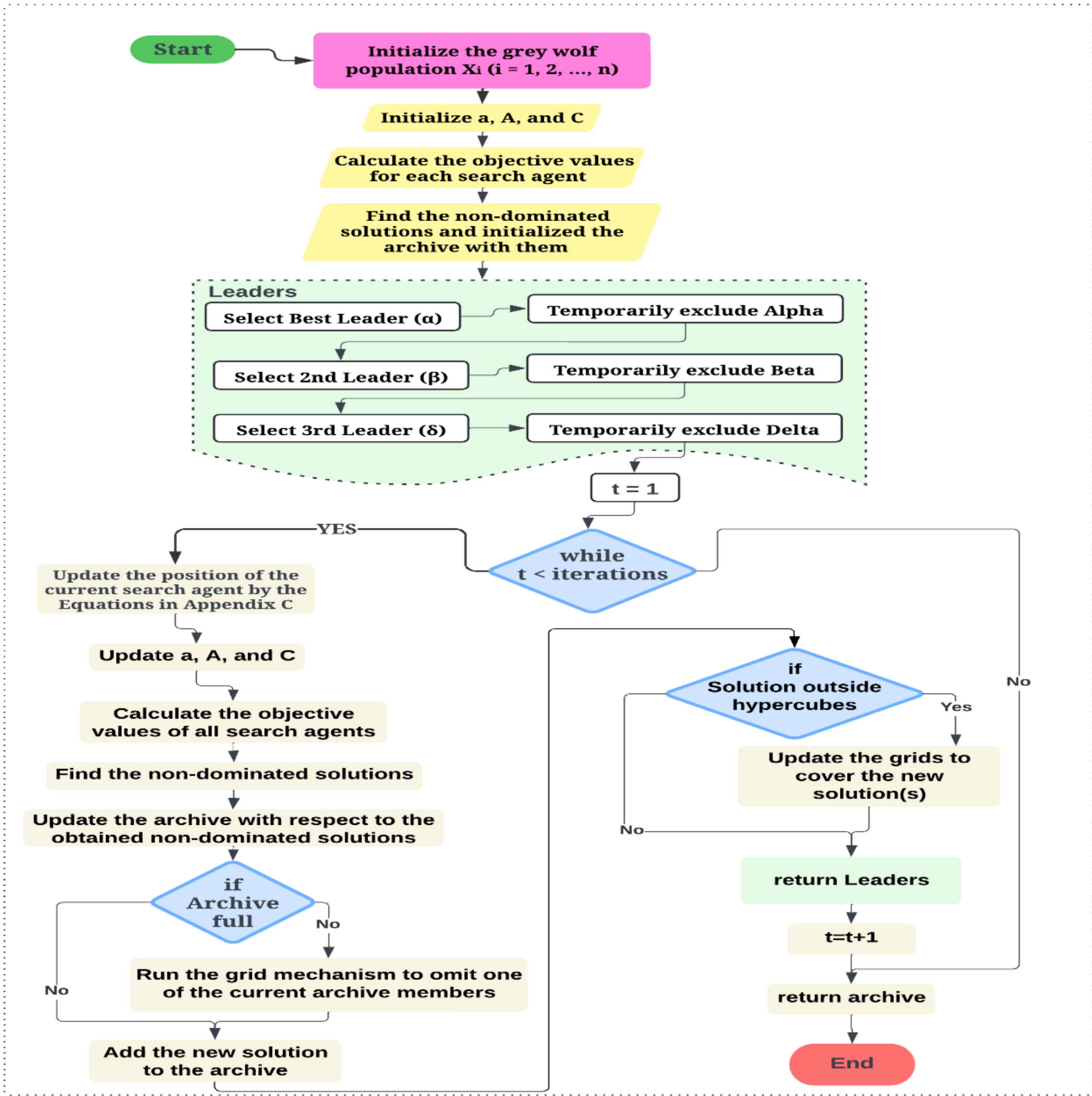

Fig. 10. General operational flowchart of the proposed MOGWOA.

The MOGWO algorithm uses simulated social leadership and encircling mechanisms to obtain the optimal solution for optimization problems. This algorithm retains the initial three best solutions acquired and directs other search agents, including omegas, to refresh their positions accordingly. The parameters a, A, and C are important in guiding the exploration process of the algorithm, as shown in Appendix C and Fig. 10. Both variables A and C are coefficient vectors, with a starting from 2 and linearly decreasing to 0 over the iterations. This decrease causes the algorithm to gradually shift its focus from exploration, which involves a broad search of the solution space, to exploitation, which involves a more focused search in the local area around the best solutions found so far. Finally, to simulate the hunting process and identify promising areas within the search space, formulas in Appendix C are executed continually for each search agent during optimization, as illustrated in Fig. 10 [54].

6.2. Multi-objective Feasibility Enhanced Particle Swarm Optimization Algorithm (MOFEPSOA)

MOFEPSOA, developed by Hasanoglu and Dolen, is a method designed for addressing multi-objective problems with constraints. It deals exclusively with inequality constraints, requiring any equality constraints to be converted into inequality constraints. The algorithm begins by initializing parameters and assessing particle positions for feasibility. If a position is feasible, it updates velocities and flight behaviours accordingly; otherwise, it adjusts them for infeasible positions. Subsequently, the algorithm rechecks the particle's new position for feasibility [56]. In this paper, MOFEPSOA will compute the objective vectors (LOCE, IR, and CO_2RA) and include the current solution in the best set. It will update the best solution in the objective vector if others do not dominate it. If the new particle position is not the best, it checks if it is not the final particle. If there are remaining iterations, MOFEPSOA repeats the previous steps from initialization. Finally, upon reaching the stopping criteria for the number of particles and iterations, MOFEPSOA presents all feasible non-dominant trade-off solutions as the Pareto front. More detailed explanations of the algorithm are presented in [57].

6.3. Employing Fuzzy Logic method for compromised Solution Identification

Many common approaches can find the best non-dominant solution, such as the fuzzy logic method. The fuzzy logic method uses the fuzzy membership function $\mu_i(F_i)$ to find the best non-dominant solution out of all non-dominant solutions stored in the archive of the MOGWOA [58]. The fuzzy membership function in (39) is used to convert each objective function (F_i) to a membership value in range between (0, 1) [59]. Where F_i^{min} and F_i^{max} represent the minimum and maximum objective function values, respectively.

$$\mu_i(F_i) = \begin{cases} 1, F_i(x) \leq F_i^{min} \\ 0, F_i(x) \geq F_i^{max} \\ \frac{F_i^{max} - F_i(x)}{F_i^{max} - F_i^{min}}, F_i^{min} \leq F_i(x) \leq F_i^{max} \end{cases} \tag{39}$$

As introduced before, this study will investigate three main scenarios. Therefore, a multi-objective optimization is performed to find three corresponding best solutions which are the reliable and affordable. Equation (40) is used to minimize $LCOE(x)$ and maximize $IR(x)$, whereas (41) is used to maximize *$CO_2RA(x)$* while minimizing $LCOE(x)$. Finally, (42) is used to minimize $LCOE(x)$ and maximize *CO_2RA*(x) and $IR(x)$ simultaneously.

$$Minimize\ F_1(x) = \left[LCOE(x), \frac{1}{IR(x)}\right] \tag{40}$$

$$Minimize\ F_2(x) = \left[\frac{1}{CO2RA(x)}, LCOE(x)\right] \tag{41}$$

$$Minimize\ F_3(x) = \left[LCOE(x), \frac{1}{IR(x)}, \frac{1}{CO2RA(x)}\right] \tag{42}$$

7. Results and Discussion

MATLAB R2022a is utilized to simulate the energy management system for the Crystal Lake territory case study. The MOGWO algorithm is employed to execute the system based on the data collected for the year 2022. The analysis includes three scenarios: the 1st scenario aims to maximize ROF (IR) whilst minimizing COF (LCOE), the 2nd scenario focuses on maximizing EOF (CO_2RA) whilst minimizing COF, and the 3rd scenario is for maximizing both ROF and EOF while minimizing COF. Accordingly, the MOFEPSOA is utilized to validate the findings obtained from MOGWOA.

7.1. Optimization using MOGWO algorithm

This study employs the MOGWOA technique to tackle the optimization problem, utilizing the mentioned decision variables of renewable components. For each scenario, a set of solutions is generated, typically amounting to around 100 solutions for each Pareto front. From this set, four essential solutions are selected and discussed, depending on the specific scenario. For instance, in the 1st scenario, the first solution, termed the reliable solution, represents the highest IR value and the highest LCOE value. The second solution known as the economic solution, exhibits the lowest IR value and the lowest LCOE value, named. The third solution, referred to as the compromised solution, lies somewhere between reliable and affordable solutions. The compromised solution is chosen based on its proximity to the origin, indicating reliability and cost-effectiveness in one aspect, and affordability and ecological sustainability in another. The Pareto frontier optimization for the 1st scenario is shown in Fig. 11.

Table 1 presents the optimization outcomes for the 1st scenario with three selected solutions, as observed in Fig. 11, detailing the objective functions of LCOE, and IR, and the decision variables N_{PV}, N_{WT}, and N_{Ht}. Notably, the optimal solution highlights the system's reliability, achieving an IR of 99.772%. However, this reliability comes at a cost, with an LCOE of 0.055708\$/kWh. Economic insights reveal that the LCOE stands at 0.04745\$/kWh, with an associated IR of 99.722% for the economic solution. Subsequently, the best solution is to install 4710 solar panels, 19 wind turbines, and 8 hydro-turbines. The chosen point aims to minimize the system's LCOE, whilst maximizing systems reliability.

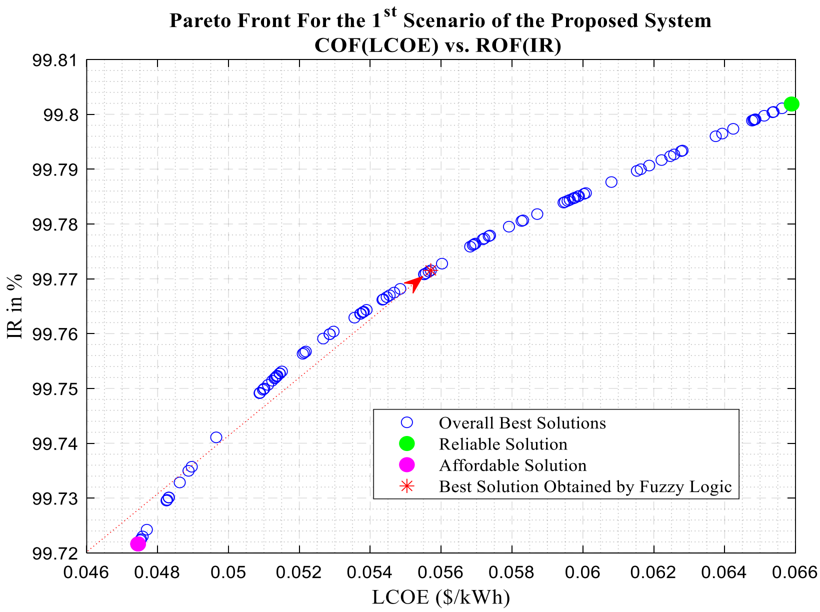

Fig. 11. Pareto Front For the 1st Scenario of the proposed system by MOGWOA.

Table 1. Optimization using MOGWOA for the 1st Scenario; COF (LCOE) vs. ROF (IR)

Quantity		COF (LCOE) vs. ROF (IR)		
		Economic	Reliable	Best Solution
Objective Functions	LCOE in \$/kWh	0.04745	0.06589	0.055708
	IR in %	99.722	99.802	99.772
Decision Variables	N_{PV}	2500	7878	4710
	N_{WT}	17	20	19
	N_{Ht}	7	9	8
Energies in GWh/year	$E_{PV\,inv}$	1.224321	3.85808	2.306623
	E_{WT}	4.711992	5.54352	5.2663443
	$E_{hydro\,turbine}$	7.2039247	6.126815	6.70430538
	E_{gsold}	0.00318518	0.52458969	0.10043583
	E_L		15.2327969	
	$E_{purchased}$	2.43467	1.0199436	1.4114235
	$E_{MHPP\,ch}$	0.096581824	0.8211559	0.3989326
Other Indicators	*LOLP in %*	3.6	1.701	2.3973
	ACS in Million \$/year	1.04597354	1.0903	0.98936
	CEA in 10^3 ton/year	1.27260922	0.61141779	0.84609526
	RSF in %	47.292	40.221	44.012

Fig. 12 illustrates the Pareto frontier optimization for the 2nd scenario implemented using MOGWOA. It aims to minimize COF (LCOE) and maximize EOF (CO_2RA). This way, it could help decision makers and design engineers who care more about environmental impacts to effectively recognize how integrating renewables could mitigate GHG emissions while minimizing the system's cost, as shown in Fig. 12.

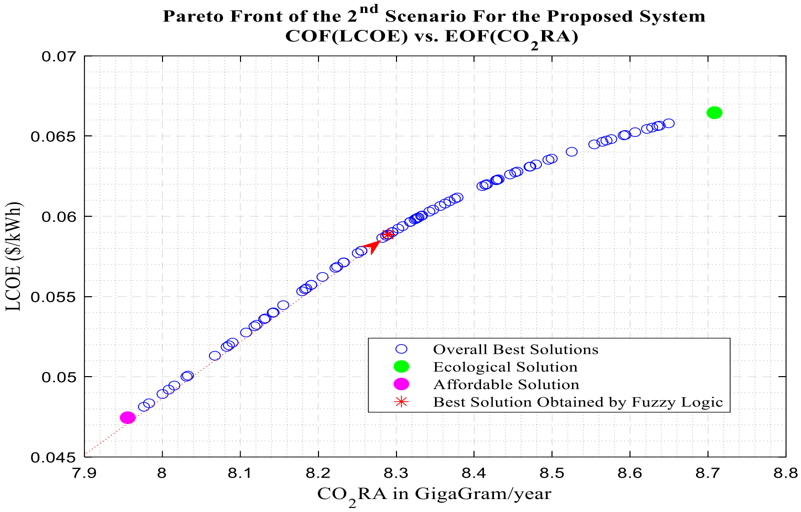

Fig. 12. Pareto Front For the 2nd Scenario of the proposed system by MOGWOA.

Table 2 shows the objective functions, decision variables, energies, and other performance indicators for the 2nd scenario. Compared with the economic and ecological cases, it can be noticed that the optimal solution achieved a compromised set of solutions, with 5639 solar panels, 19 wind turbines, and 8 hydro-turbines. Additionally, the findings are close to those obtained using the 1st scenario, which proves the effectiveness of the optimization algorithm and the proposed methodology.

Table 2. Optimization using MOGWOA for the 2nd Scenario; COF (LCOE) vs. EOF (CO_2RA)

Quantity		COF (LCOE) vs. EOF (CO_2RA)		
		Economical	Ecological	Best Solution
Objective Functions	LCOE in \$/kWh	0.04911	0.066457	0.059181
	CO_2RA in 10^3 ton/year	8.0056	8.7082	8.3008
Decision Variables	N_{PV}	2964	8150	5639
	N_{WT}	18	20	19
	N_{Ht}	7	9	8
Energies in GWh	$E_{PV\,inv}$	1.4515561	3.991289	2.7615806
	E_{WT}	4.9891683	5.5435203	5.2663443
	$E_{hydro\,turbine}$	6.9300397	6.085227	1.35779573
	E_{gsold}	0.01125435	0.5805854	0.17126333
	E_L		15.2327969	
	$E_{purchased}$	2.00571	1.01293624	1.35779573
	$E_{MHPP\,ch}$	0.1965026	0.84950283	0.47434083
Other Indicators	*LOLP in %*	3.3904	1.7009	2.2945
	ACS in Million \$/year	1.0482	1.1054	1.051
	CEA in 10^3 ton/year	1.202346	0.6072172	0.81394744
	RSF in %	45.494	39.948	42.352

In this paper, modified triple objective functions are employed to enhance the simulation and accuracy of the proposed system. This approach is uncommon in similar studies as it incorporates three objective functions (reliability, ecological, and economic) into a triple Pareto frontier analysis, as illustrated in Table 3 and Fig. 13. Existing research typically focuses on two objective functions, making this method distinct in its comprehensive consideration of all three aspects simultaneously.

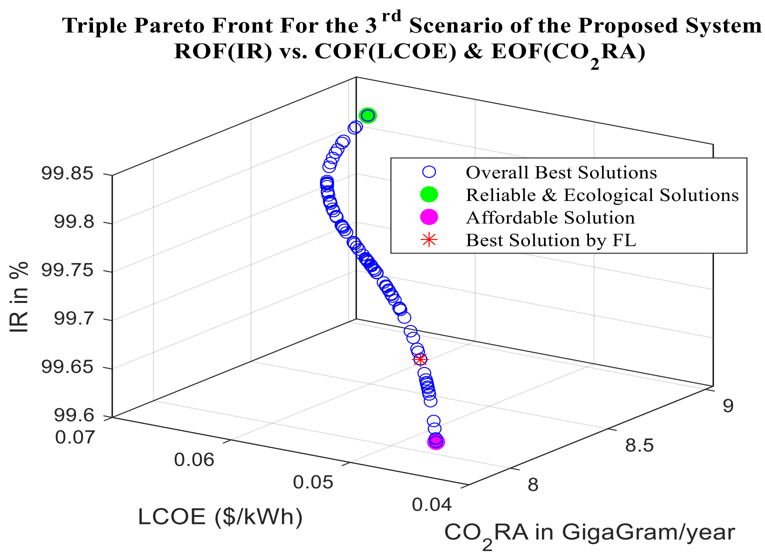

Fig. 13. Triple Pareto Front For the 3rd Scenario of the proposed system using MOGWOA.

Table 3. Optimization using MOGWOA for the 3rd Scenario: Triple Objective Functions "ROF (IR) vs. COF (LCOE) & EOF (CO_2RA)"

Quantity		ROF (IR) vs. COF (LCOE) & EOF (CO_2RA)			
		Economic	Reliable	Ecological	Best Solution
Objective Functions	IR in %	99.638	99.812	99.812	99.705
	LCOE in $/kWh	0.042771	0.069025	0.069025	0.046147
	CO_2RA in *10^3 ton/year*	7.7887	9.0393	9.0393	7.9142
Decision Variables	N_{PV}	2052	9823	9823	5124
	N_{WT}	17	20	20	19
	N_{Ht}	7	9	9	8
Storage Capacity in GWh		14.9734			
n_{day} in days		8807			
Energies in GWh	$E_{PV_{inv}}$	1.00492347	4.81060586	4.81060586	2.50937
	E_{WT}	4.71199224	5.54352	5.54352	5.2663443
	$E_{hydro_{turbine}}$	7.31769778	5.86857699	5.86857699	6.5881848
	$E_{purchased}$	2.20215013	0.9769594	0.9769594	1.3859264
	E_{gsold}	0.00141861	0.99834236	0.99834236	0.12942049
	E_L	15.232796912			
	$E_{MHPP_{ch}}$	0.076158288	0.99708479	0.99708479	0.42996824
Other Indicators	$LOLP$ *in %*	3.6872	1.6324	1.6324	2.3516
	ACS *in Million \$/year*	1.0303	1.1877	1.1877	1.0167
	CEA *in 10^3 ton/year*	1.32010613	0.58565	0.58565	0.830810725
	RSF *in %*	48.039	38.526	38.526	43.25

The blue circles represent the candidate solutions, while the green circle highlights a solution that is both reliable and ecological, with the values of 99.812% and 0.069025 × 10^3 ton/year, respectively, as outlined in Table 3. This is because the algorithms aim to maximize both IR and CO_2RA. However, the cost is taken into account with a minimum economic LCOE of 0.042771\$/kWh. Upon closer examination of Table 3, it becomes evident that the fuzzy logic approach yields the optimal solution among the economic, reliable, and ecological objective functions. This optimal solution achieves an IR of 99.705%, a LCOE of 0.046147 \$/kWh, and a CO_2RA of 7.9142 ×10^3 ton/year. The associated decision variables are N_{PV}= 5124, N_{WT}=19, and N_{Ht} = 8.

7.2. Power computation analysis

Once the objective functions, decision variables, energy values, and other system indicators are determined for each scenario outlined in section 7.1, an evaluation of the system's performance in the 3rd scenario will be provided in this section. Fig. 14 illustrates how much renewable power could be generated monthly throughout 2022. It reveals the contributions from solar PV, wind, and hydro energy resources, showing their combined generated power. Each month is visible along the horizontal axis, with the amount of power generated in MW, shown on the vertical axis. This visualization helps us understand patterns in renewable energy production over the year, revealing any seasonal fluctuations and emphasizing the importance of each renewable energy source in sufficiently meeting the load demand.

Solar PV is chosen from renewable resources to show the average monthly output power for the year 2022, shown in Fig. 15. From the graph, it is evident that the highest PV output occurs between April and August, coinciding with periods of increased solar irradiance during these months. Conversely, the lowest average PV output power is observed in winter, corresponding to times when solar irradiance is comparatively lower in Michigan. This highlights the influence of seasonal variations in solar irradiance on PV power generation throughout the year.

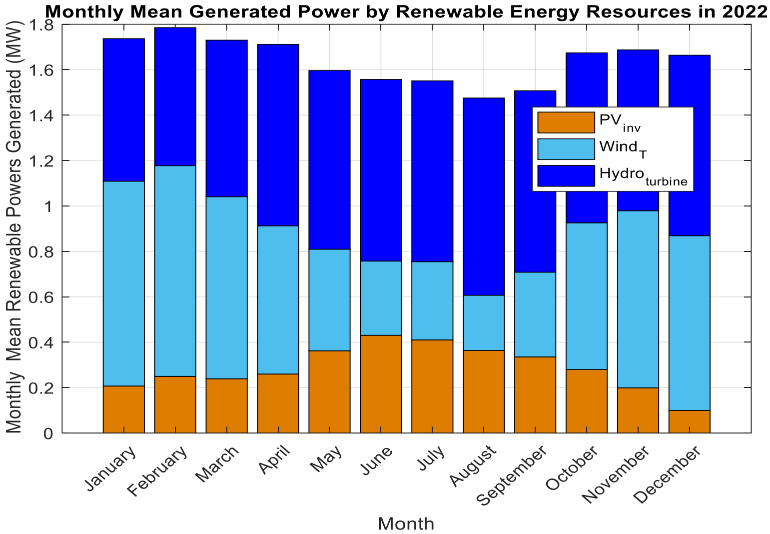

Fig. 14. The monthly mean generated power by renewable energy resources of the 3rd scenario in MW.

The average purchased and sold power from and to the grid and the pumping power to UCL for each month are depicted in Fig. 16. It presents the performance in the best case of the third scenario. The plot effectively visualizes the monthly trends in power generation, with distinct lines representing grid-purchased power, grid-sold power, and pumping power. It is noticeable that grid-purchased power exhibits fluctuations throughout the year, with higher values observed after September till the end of the year, possibly indicative of increased energy demand during winter. On the other hand, the grid-sold power shows relatively consistent levels across the months because of the priority of the extra power being pumped to the UCL. Overall, the visualization offers valuable insights into the dynamics of power generation and consumption for the year, providing useful information for energy management and decision-making.

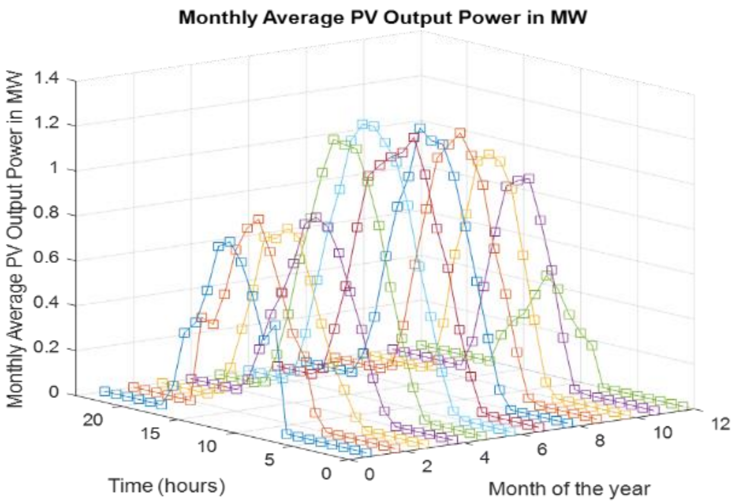

Fig. 15. The monthly average solar PV output power for the best solution of the 3rd scenario in MW.

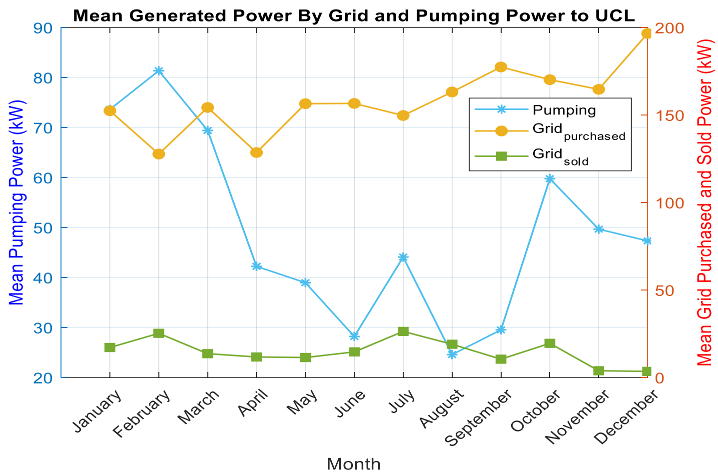

Fig. 16. Average generated power by grid and pumping power to UCL in each month for the best case of the 3rd scenario.

Fig. 17 states the findings of the operational strategy simulation for the optimized 3rd scenario, focusing on a summer day, specifically July 1st, 2022. One notable observation is the absence of hydro pumping during nighttime hours, attributed to the lack of solar PV power availability. During the daytime, typically between 10:00 A.M. and 4:00 P.M., the solar and wind-generated power meets the load demand, with excess energy utilized for pumping water from the lower reservoir to the UCL. Additionally, it is highlighted that the energy balance equation is maintained in each scenario, as described previously in equation (29). Subsequently, around 2:00 P.M., the total load demand, sold, and pumping power comprises the energy supplied by both the PV system and the wind plant, with zero purchased power since the grid serves as a backup source in instances of renewable energy deficit.

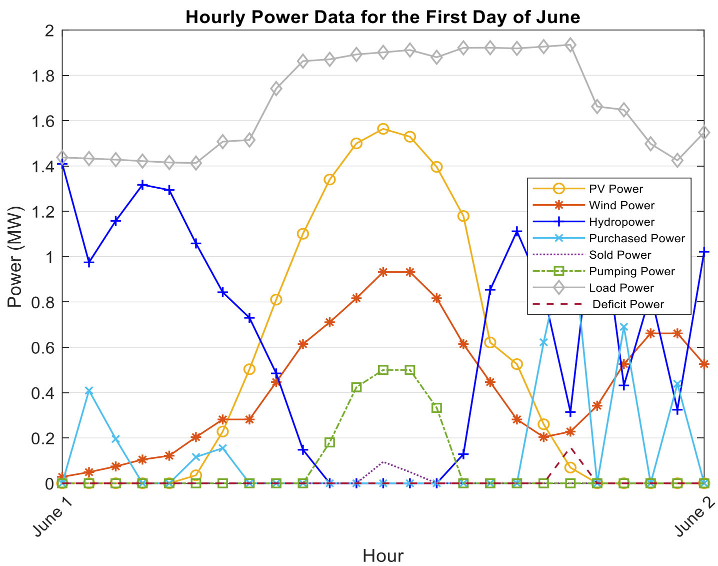

Fig. 17. Hourly power data for June, 1st 2022 for the optimal case of the 3rd scenario.

7.3. Comparative analysis of findings using MOFEPSOA

In this section, a comparative analysis of the findings in Section 7.1 is carried out using MOFEPSOA to test the effectiveness of MOGWOA. By comparing the results obtained previously, the performance of MOGWOA can be assessed. The Pareto fronts of the 1st and 2nd scenarios are shown in Fig. 18.

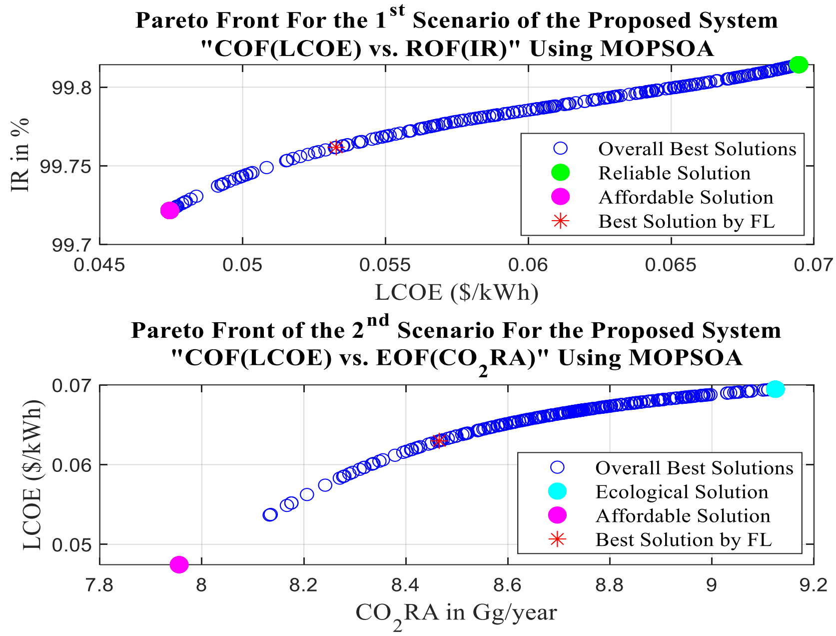

Fig. 18. Pareto fronts for the 1st and 2nd scenarios of the proposed system by MOFEPSOA.

Table 4 displays the objective function values and decision variables for the 3rd scenario obtained using MOFEPSOA. The percentage difference between MOGWOA and MOFEPSOA is consistently below 7% for all values, particularly compared with the findings in the optimal solution of Table 3. Moreover, the triple Pareto front optimization curve produced by MOFEPSOA closely aligns with MOGWOA's results in Fig. 19, affirming the accuracy and effectiveness of the proposed methodology in simulating the system.

Table 4. Comparative analysis for the 3rd Scenario using MOFEPSOA based on MOGWOA findings.

Quantity		ROF (IR) vs. COF (LCOE) & EOF (CO_2RA)			
		Using MOFEPSOA			Percentage difference for Best Solution from MOGWOA in %
		Economic	Reliable & Ecological	Best Solution	
Objective Functions	IR in %	99.722	99.814	99.739	0.09
	LCOE in $/kWh	0.04745	0.069464	0.049348	6.704
	CO_2RA in *10^3 ton/year*	7.9556	9.1243	8.0124	1.23
Decision Variables	N_{PV}	2117	10251	5029	1.8714
	N_{WT}	17	19	20	5.128
	N_{Ht}	8	9	8	0

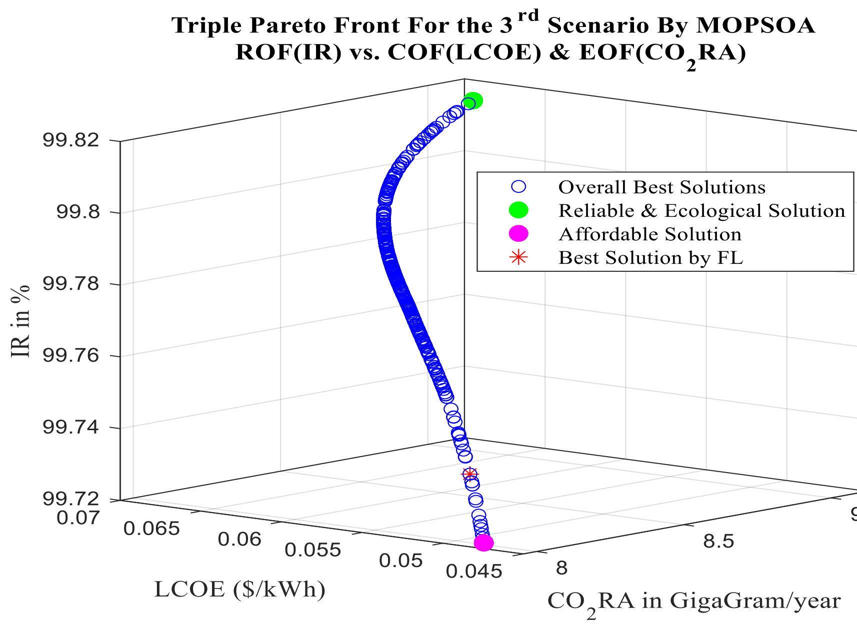

Fig. 19. Triple Pareto Front For the 3rd Scenario of the proposed system using MOFEPSOA.

8. Conclusions

Recently, with growing electricity demand and increasing ecological concerns, the significance of RERs, including hydro storage systems, has become increasingly apparent. This has made a global shift towards cleaner and more sustainable energy alternatives to replace conventional fossil fuel infrastructure with clean, affordable, and reliable options. This has inspired this paper to investigate renewable energy resource concerns, painting the maximum reliability, maximum emission reduction, and minimum systems' lifetime cost. This paper examines the utilization of on-grid solar PV, wind farms, and PHESS to meet the energy needs of Crystal's Lake territory in Michigan as a case study. A realistic analysis was conducted using measured data for the system's design from the year 2022, including solar data, ambient temperature, wind velocity, hydrological information, and community-scale energy demand specific to the chosen location. The primary objective is to assess the potential of untapped sites for renewable energy generation, with Crystal's Lake identified as particularly promising due to its substantial storage capacity of about 14.9734 GWh, despite being classified as a MHPP. Through the application of a MOGWOA, optimal sizing, and energy management strategies were formulated for various scenarios. Economic, environmental, and reliability criteria were utilized as the three objective functions, yielding promising outcomes, particularly in the third scenario where triple objective functions were considered. For each scenario, multiple solutions were identified, including economic, ecological, reliable, and a best-compromised solution achieved through a fuzzy logic approach. Notably, the third scenario yielded the lowest LCOE at 0.046147 $/kWh, a strong index of reliability of 99.705%, and a significant reduction in CO_2 emissions by 7.9142 10^3 tons per year. This scenario also revealed the optimum number of solar panels was 5124, 19 wind turbines, and 8 hydro-turbine generator sets. Furthermore, the renewable storage factor was determined to be 43.25%, indicating optimal utilization of available PHESS. Energy management analysis further validated the efficacy of the system. Subsequently, the findings were validated using a MOFEPSOA, ensuring accuracy with a percentage difference lower than 7% across all results. The approach described in this research offers valuable perspectives for comparable locations aiming to utilize renewable energy, specifically from unused storage reservoirs. By optimizing the integration of RES, this research offers a roadmap for maximizing the utilization of clean energy sources and promoting a more sustainable future.

Appendix A

TABLE 5. Specifications of Renewable Components

Component	Parameters	Value
Solar PV Module (CanadianSolar CS6K-290MS)	*Maximum power (P_{max}) in Watt*	*290*
	Module Efficiency STC in %	*17.72 %*
	Short circuit current (I_{sc}) in A	*9.67*
	Open circuit voltage (V_{oc}) in V	*39.3*
	Maximum power current (I_{MPP}) in A	*9.05*
	Maximum power voltage (V_{MPP}) in V	*32.1*
	Temperature coefficient of V_{oc} in %/℃	*-0.3*
	Temperature coefficient of I_{sc} in %/℃	*0.053*
	NOCT (°C)	*45*
	$T_{MDS,STC}$ in ℃	*20*
	GTI_{NOCT} in Watt/m²	*800*
	Dimensions for Area ($L_m \times W_m$) in m²	*1.65×0.992*
Wind Turbine (Vestas V200-100 kW)	*Nominal Power*	*100 kW*
	Frequency	*50 Hz*
	Diameter	*20 m*
	Swept Area	*314.0 m²*
	Hub height	*40 m*
	Cut-in Wind Speed (v_{ci})	*3.3 m/s*
	Rated Wind Speed (v_r)	*13 m/s*
	Cut-out Wind Speed (v_{co})	*25 m/s*
Upper Crystal Lake Dimensions [26]	*Average Lake width ($\overline{W}_{UCL}$)*	*3.12 km*
	Elevation	*183 m*
	Difference from Lake Michigan (H_{diff})	*0.8 km*
	Average Lake length ($\overline{L}_{UCL}$)	*12.87 km*
	Average depth ($\overline{D}_{UCL}$)	*21.55 m*

Appendix B

TABLE 6. Financial data for LCOE computation

Cost type	PV array [60]	Wind farm [60]	PHS facility [61]	Converter [61]
CC ($/kW)	896	998	930	687
OMC ($/kW.year)	15	20	15.52	687
RC ($/kW)	896	998	930	0
Lifetime (years)	25	20	25	15
Grid costs				
E_{gp} Cost ($/kWh)	0.37			

E_{gsold} Cost ($/kWh) [62]	0.176
Financial Parameters	
i' (%)	8
$f_{inflation}$ (%)	2
Project lifetime (N)	
25	

Appendix C

$$\vec{D} = \left|\vec{C} \,.\, \vec{X}_p(t) \; - \; \vec{X}(t)\right| \tag{43}$$

$$\vec{X}(t+1) = \vec{X}_p(t) - \vec{A} \,.\, \vec{D} \tag{44}$$

$$\vec{A} = 2\vec{a} \,.\, \vec{r}_1 - \vec{a} \tag{45}$$

$$\vec{C} = 2 \,.\, \vec{r}_2 \tag{46}$$

$$\vec{D}_\alpha = \left|\vec{C}_1 \,.\, \vec{X}_\alpha \; - \; \vec{X}\right| \tag{47}$$

$$\vec{D}_\beta = \left|\vec{C}_2 \,.\, \vec{X}_\beta \; - \; \vec{X}\right| \tag{48}$$

$$\vec{D}_\delta = \left|\vec{C}_3 \,.\, \vec{X}_\delta \; - \; \vec{X}\right| \tag{49}$$

$$\vec{X}_1 = \vec{X}_\alpha \; - \; \vec{A}_1 \,.\, (\vec{D}_\alpha) \tag{50}$$

$$\vec{X}_2 = \vec{X}_\beta \; - \; \vec{A}_2 \,.\, (\vec{D}_\beta) \tag{51}$$

$$\vec{X}_3 = \vec{X}_\delta \; - \; \vec{A}_3 \,.\, (\vec{D}_\delta) \tag{52}$$

$$\vec{X}(t+1) = \frac{\vec{X}_1 + \vec{X}_2 + \vec{X}_3}{3} \tag{53}$$

Acknowledgment

This work was supported in part by the National Science Foundation of USA under Grant ECCS-2146615 and partially supported by the Department of Energy, Solar Energy Technologies Office (SETO) Renewables Advancing Community Energy Resilience (RACER) program under Award Number DE-EE0010413. Any opinions, findings, conclusions, or recommendations expressed in this material are those of the authors and do not necessarily reflect the views of the Department of Energy.

References

[1] A. Valavanidis, "Global Electricity Generation from Renewable Sources."

[2] O. M. Babatunde, J. L. Munda, and Y. Hamam, "A comprehensive state-of-the-art survey on hybrid renewable energy system operations and planning," IEEE Access, vol. 8, pp. 75313-75346, 2020.

[3] J. E. Breck, "Compilation of databases on Michigan lakes," 2013.

[4] A. Berrada, Z. Bouhssine, and A. Arechkik, "Optimisation and economic modeling of micro hydropower plant integrated in water distribution system," Journal of cleaner production, vol. 232, pp. 877-887, 2019.

[5] H. D. Laksono and R. Fahreza, "Optimal Sizing of Micro Hydropower to Improve Hybrid Renewable Power System," in 2020 7th International Conference on Electrical Engineering, Computer Sciences and Informatics (EECSI), 2020: IEEE, pp. 95-99.

[6] M. I. Abid, M. S. Khalid, M. Kamran, M. A. Rasheed, M. F. Masood, and T. Murtaza, "Design and optimization of the micro-hydro power system for remote areas of Pakistan," International Journal of Smart Grid-ijSmartGrid, vol. 4, no. 3, pp. 125-138, 2020.

[7] F. A. Canales and A. Beluco, "Modeling pumped hydro storage with the micropower optimization model (HOMER)," Journal of renewable and sustainable energy, vol. 6, no. 4, 2014.

[8] A. Tapia, D. Reina, and P. Millán, "Optimized micro-hydro power plants layout design using messy genetic algorithms," Expert Systems with Applications, vol. 159, p. 113539, 2020.

[9] B. Dye, "Stiegler's Gorge Dam, Tanzania," 2019.

[10] G. E. Alvarez, "Operation of pumped storage hydropower plants through optimization for power systems," Energy, vol. 202, p. 117797, 2020.

[11] M. Shabani, E. Dahlquist, F. Wallin, and J. Yan, "Techno-economic comparison of optimal design of renewable-battery storage and renewable micro pumped hydro storage power supply systems: A case study in Sweden," Applied Energy, vol. 279, p. 115830, 2020.

[12] H. M. Al-Masri, S. K. Magableh, A. Abuelrub, and K. Alzaareer, "Realistic coordination and sizing of a solar array combined with pumped hydro storage system," Journal of Energy Storage, vol. 41, p. 102915, 2021.

[13] M. Petrollese, P. Seche, and D. Cocco, "Analysis and optimization of solar-pumped hydro storage systems integrated in water supply networks," Energy, vol. 189, p. 116176, 2019.

[14] M. Jaszczur, Q. Hassan, P. Palej, and J. Abdulateef, "Multi-Objective optimisation of a micro-grid hybrid power system for household application," Energy, vol. 202, p. 117738, 2020.

[15] A. Tapia, A. del Nozal, D. Reina, and P. Millán, "Three-dimensional optimization of penstock layouts for micro-hydropower plants using genetic algorithms," Applied Energy, vol. 301, p. 117499, 2021.

[16] M. Sengupta, Y. Xie, A. Lopez, A. Habte, G. Maclaurin, and J. Shelby, "The national solar radiation data base (NSRDB)," Renewable and sustainable energy reviews, vol. 89, pp. 51-60, 2018.

[17] A. El-Sebaii, F. Al-Hazmi, A. Al-Ghamdi, and S. J. Yaghmour, "Global, direct and diffuse solar radiation on horizontal and tilted surfaces in Jeddah, Saudi Arabia," Applied energy, vol. 87, no. 2, pp. 568-576, 2010.

[18] H. M. Al-Masri, S. K. Magableh, and A. Abuelrub, "Output power computation and sizing of a photovoltaic array by advanced modeling," Sustainable Energy Technologies and Assessments, vol. 47, p. 101519, 2021.

[19] Solarific. "Solar Panel Angles for Benzonia, Michigan, US." https://solarific.co/us/mi/detroit (accessed Jan, 9 2024).

[20] H. M. K. Al-Masri, O. M. Dawaghreh, and S. K. Magableh, "Realistic performance evaluation and optimal energy management of a large-scale bifacial photovoltaic system," Energy Conversion and Management, vol. 286, p. 117057, 2023/06/15/ 2023, doi: https://doi.org/10.1016/j.enconman.2023.117057.

[21] M. Fengler. "Energy Forecasts for Wind, Weather API." https://www.meteomatics.com/ (accessed Jan, 29 2024).

[22] A. Vasel-Be-Hagh and C. L. Archer, "Wind farm hub height optimization," Applied energy, vol. 195, pp. 905-921, 2017.

[23] P. L. Storck, Journey to the Ice Age: discovering an ancient world. UBC Press, 2004.

[24] S. L. Daniels, "Inland Lakes Levels Matter."

[25] S. L. Daniels, "The History of Crystal Lake Water Levels ", 2016. Accessed: (accessed Jan, 9 2024). [Online]. Available: https://shorturl.at/zDQZ3

[26] R. Cosaro. "Watershed Facts. The Crystal Lake Watershed Association (CLWA)." https://crystallakewatershed.org/watershed-facts/ (accessed Jan, 9 2024).

[27] L. W. Devin Hampton, Daniel Roesler. "Utility Data API, UtilityAPI." https://utilityapi.com/products#api (accessed Feb, 5 2024.

[28] K. Ishaque, Z. Salam, and H. Taheri, "Simple, fast and accurate two-diode model for photovoltaic modules," Solar energy materials and solar cells, vol. 95, no. 2, pp. 586-594, 2011.

[29] G. Cerofolini and M. Polignano, "Generation-recombination phenomena in almost ideal silicon p-n junctions," Journal of applied physics, vol. 64, no. 11, pp. 6349-6356, 1988.

[30] S. S. Hegedus and A. Luque, "Status, trends, challenges and the bright future of solar electricity from photovoltaics," Handbook of photovoltaic science and engineering, pp. 1-43, 2003.

[31] K. Ishaque, Z. Salam, and H. Taheri, "Accurate MATLAB simulink PV system simulator based on a two-diode model," Journal of Power Electronics, vol. 11, no. 2, pp. 179-187, 2011.

[32] V. J. Chin, Z. Salam, and K. Ishaque, "An accurate modelling of the two-diode model of PV module using a hybrid solution based on differential evolution," Energy conversion and management, vol. 124, pp. 42-50, 2016.

[33] F. Attivissimo, F. Adamo, A. Carullo, A. M. L. Lanzolla, F. Spertino, and A. Vallan, "On the performance of the double-diode model in estimating the maximum power point for different photovoltaic technologies," Measurement, vol. 46, no. 9, pp. 3549-3559, 2013.

[34] T. Ma, H. Yang, L. Lu, and J. Peng, "Pumped storage-based standalone photovoltaic power generation system: Modeling and techno-economic optimization," Applied energy, vol. 137, pp. 649-659, 2015.

[35] N. Mohammad, M. Islam, T. Karim, and Q. D. Hossain, "Improved Solar Photovoltaic Array Model with FLC Based Maximum Power Point Tracking," International Journal of Electrical & Computer Engineering (2088-8708), vol. 2, no. 6, 2012.

[36] Z. Jing, J. Zhu, R. J. J. o. M. P. S. Hu, and C. Energy, "Sizing optimization for island microgrid with pumped storage system considering demand response," vol. 6, no. 4, pp. 791-801, 2018.

[37] T. Ma, H. Yang, L. Lu, and J. J. R. e. Peng, "Technical feasibility study on a standalone hybrid solar-wind system with pumped hydro storage for a remote island in Hong Kong," vol. 69, pp. 7-15, 2014.

[38] H. Ibrahim, A. Ilinca, and J. Perron, "Energy storage systems—Characteristics and comparisons," Renewable and sustainable energy reviews, vol. 12, no. 5, pp. 1221-1250, 2008.

[39] A. Franco and F. Donatini, "Methods for the estimation of the energy stored in geothermal reservoirs," in Journal of Physics: Conference Series, 2017, vol. 796, no. 1: IOP Publishing, p. 012025.

[40] H. M. Al-Masri, A. A. Al-Sharqi, S. K. Magableh, A. Q. Al-Shetwi, M. G. Abdolrasol, and T. S. Ustun, "Optimal allocation of a hybrid photovoltaic biogas energy system using multi-objective feasibility enhanced particle swarm algorithm," Sustainability, vol. 14, no. 2, p. 685, 2022.

[41] H. M. Al-Masri, S. K. Magableh, A. Abuelrub, O. Saadeh, and M. Ehsani, "Impact of different photovoltaic models on the design of a combined solar array and pumped hydro storage system," Applied Sciences, vol. 10, no. 10, p. 3650, 2020.

[42] A. D. BANK, "Guidelines for estimating greenhouse gas emissions of Asian Development Bank projects: Additional guidance for clean energy projects," Philippines, 2017. [Online]. Available: http://dx.doi.org/10.22617/TIM178659-2

[43] "EPA greenhouse gas reporting and emission rates." https://www.uppermichiganenergy.com/regulation/energymix-emissionrates.htm (accessed on 4 Nov 2023) (accessed.

[44] H. M. Al-Masri, O. M. Dawaghreh, and S. K. Magableh, "Optimal configuration of a large scale on-grid renewable energy systems with different design strategies," Journal of Cleaner Production, p. 137572, 2023.

[45] H. F. Boroujeni, M. Eghtedari, M. Abdollahi, and E. Behzadipour, "Calculation of generation system reliability index: Loss of Load Probability," Life Science Journal, vol. 9, no. 4, pp. 4903-4908, 2012.

[46] U. J. U. D. o. E. W. EIA, DC, USA, "US Energy Information Administration Annual Energy Outlook 2020," 2020.

[47] M. S. Javed, D. Zhong, T. Ma, A. Song, and S. Ahmed, "Hybrid pumped hydro and battery storage for renewable energy based power supply system," Applied Energy, vol. 257, p. 114026, 2020.

[48] X. Lu, X. Pu, and X. Han, "Sustainable smart waste classification and collection system: a bi-objective modeling and optimization approach," Journal of Cleaner Production, vol. 276, p. 124183, 2020.

[49] M. Neshat et al., "Enhancing the performance of hybrid wave-wind energy systems through a fast and adaptive chaotic multi-objective swarm optimisation method," Applied Energy, vol. 362, p. 122955, 2024.

[50] M. Seifpour, S. A. Asghari, and M. Ghobaei-Arani, "A stochastic multi-objective optimization method for railways scheduling: a NSGA-II-based hybrid approach," The Journal of Supercomputing, vol. 80, no. 2, pp. 2128-2163, 2024.

[51] S. Gürgen and İ. Altın, "Novel decision-making strategy for working fluid selection in Organic Rankine Cycle: A case study for waste heat recovery of a marine diesel engine," Energy, vol. 252, p. 124023, 2022.

[52] A. Shukla, K. Verma, and R. Kumar, "Multi-objective synergistic planning of EV fast-charging stations in the distribution system coupled with the transportation network," IET Generation, Transmission & Distribution, vol. 13, no. 15, pp. 3421-3432, 2019.

[53] D. Yousri, S. B. Thanikanti, K. Balasubramanian, A. Osama, and A. Fathy, "Multi-objective grey wolf optimizer for optimal design of switching matrix for shaded PV array dynamic reconfiguration," IEEE Access, vol. 8, pp. 159931-159946, 2020.

[54] S. Mirjalili, S. Saremi, S. M. Mirjalili, and L. d. S. Coelho, "Multi-objective grey wolf optimizer: a novel algorithm for multi-criterion optimization," Expert systems with applications, vol. 47, pp. 106-119, 2016.

[55] S. N. Makhadmeh, O. A. Alomari, S. Mirjalili, M. A. Al-Betar, and A. Elnagar, "Recent advances in multi-objective grey wolf optimizer, its versions and applications," Neural Computing and Applications, vol. 34, no. 22, pp. 19723-19749, 2022.

[56] M. S. Hasanoğlu, "An Advanced evolutionary programming method for mechanical system design: feasibility enhanced

particle swarm optimization," 2019.

[57] M. Sinan Hasanoglu and M. Dolen, "Multi-objective feasibility enhanced particle swarm optimization," Engineering Optimization, vol. 50, no. 12, pp. 2013-2037, 2018.

[58] B. M. Kalesar, B. Rouhollahi, J. B. Noshahr, M. Tadayon, and M. Kermani, "Multi-Objective Fuzzy Model for Optimal Siting and Sizing of DG Units to Reduce Losses Using Genetic Algorithm," in 2018 IEEE International Conference on Environment and Electrical Engineering and 2018 IEEE Industrial and Commercial Power Systems Europe (EEEIC/I&CPS Europe), 2018: IEEE, pp. 1-6.

[59] M. I. Alomoush, "Microgrid combined power-heat economic-emission dispatch considering stochastic renewable energy resources, power purchase and emission tax," Energy Conversion and Management, vol. 200, p. 112090, 2019.

[60] M. S. Javed et al., "Economic analysis and optimization of a renewable energy based power supply system with different energy storages for a remote island," vol. 164, pp. 1376-1394, 2021.

[61] N. Yimen, O. Hamandjoda, L. Meva'a, B. Ndzana, and J. J. E. Nganhou, "Analyzing of a photovoltaic/wind/biogas/pumped-hydro off-grid hybrid system for rural electrification in Sub-Saharan Africa—Case study of Djoundé in Northern Cameroon," vol. 11, no. 10, p. 2644, 2018.

[62] E. C. Okonkwo, C. F. Okwose, and S. J. I. J. o. R. E. R. Abbasoglu, "Techno-economic analysis of the potential utilization of a hybrid PV-wind turbine system for commercial buildings in Jordan," vol. 7, no. 2, pp. 908-914, 2017.